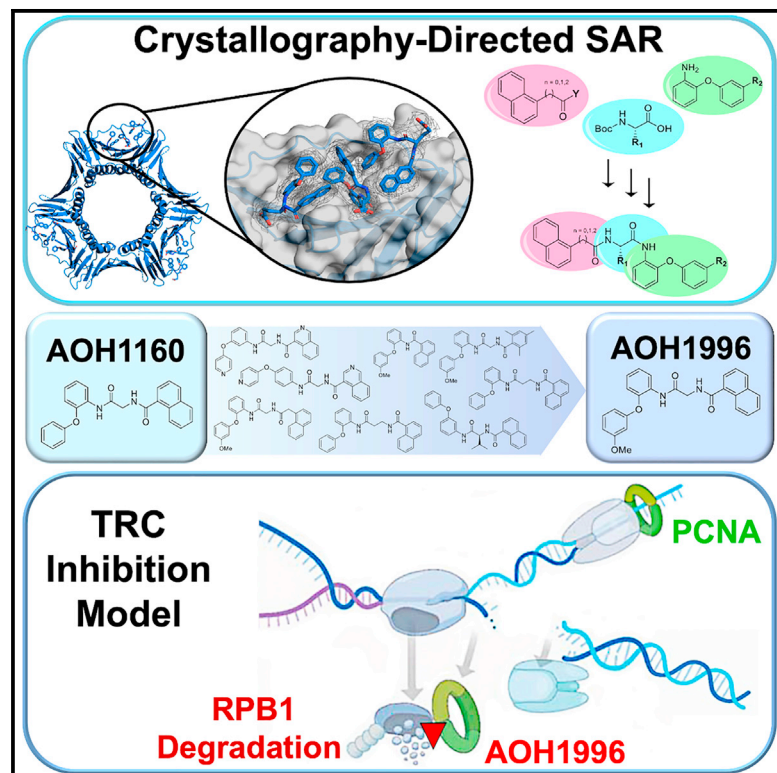


Cell Chemical Biology

Small molecule targeting of transcription-replication conflict for selective chemotherapy

Graphical abstract



Authors

Long Gu, Min Li, Caroline M. Li, ..., Robert J. Hickey, J. Jefferson P. Perry, Linda H. Malkas

Correspondence

Lgu@coh.org

In brief

Gu et al. used crystallography-directed medicinal chemistry to identify a small molecule ligand of PCNA that interferes with the resolution of transcription-replication conflicts. This compound was found to be orally active and inhibited tumor growth in animals without causing any discernable toxicity even at 6 times its effective dose.

Highlights

- Crystallography-directed medicinal chemistry identifies a PCNA ligand (AOH1996)
- AOH1996 enhances PCNA and RPB1 interaction and interferes with TRC resolution
- AOH1996 induces DNA double-stranded breaks in a transcription dependent manner
- Given orally, AOH1996 suppresses tumor growth but causes no discernable side effect

Article

Small molecule targeting of transcription-replication conflict for selective chemotherapy

Long Gu,^{1,*} Min Li,² Caroline M. Li,¹ Pouya Haratipour,³ Robert Lingeman,¹ Jennifer Jossart,¹ Margarita Gutova,⁴ Linda Flores,⁴ Caitlyn Hyde,⁴ Nikola Kenjić,⁵ Haiqing Li,⁶ Vincent Chung,⁷ Hongzhi Li,⁸ Brett Lomenick,⁹ Daniel D. Von Hoff,¹⁰ Timothy W. Synold,¹¹ Karen S. Aboody,⁴ Yilun Liu,² David Horne,³ Robert J. Hickey,³ J. Jefferson P. Perry,¹ and Linda H. Malkas^{1,12}

¹Department of Molecular Diagnostics & Experimental Therapeutics, Beckman Research Institute of City of Hope, Duarte, CA, USA

²Department of Cancer Genetics and Epigenetics, Beckman Research Institute of City of Hope, Duarte, CA, USA

³Department of Cancer Biology & Molecular Medicine, Beckman Research Institute of City of Hope, Duarte, CA, USA

⁴Department of Developmental & Stem Cell Biology, Beckman Research Institute of City of Hope, Duarte, CA, USA

⁵Department of Biochemistry, University of California Riverside, Riverside, CA, USA

⁶Department of Genomics, Beckman Research Institute of City of Hope, Duarte, CA, USA

⁷Department of Medical Oncology, City of Hope, Duarte, CA, USA

⁸Department of Bioinformatics, Beckman Research Institute of City of Hope, Duarte, CA, USA

⁹Proteome Exploration Laboratory, California Institute of Technology, Pasadena, CA, USA

¹⁰Clinical Translational Research Division, Translational Genomics Research Institute, 445N 5th Street, Phoenix, AZ 85004, USA

¹¹Department of Medical Oncology and Therapeutics Research, Beckman Research Institute of City of Hope, Duarte, CA, USA

¹²Lead contact

*Correspondence: Lgu@coh.org

<https://doi.org/10.1016/j.chembiol.2023.07.001>

SUMMARY

Targeting transcription replication conflicts, a major source of endogenous DNA double-stranded breaks and genomic instability could have important anticancer therapeutic implications. Proliferating cell nuclear antigen (PCNA) is critical to DNA replication and repair processes. Through a rational drug design approach, we identified a small molecule PCNA inhibitor, AOH1996, which selectively kills cancer cells. AOH1996 enhances the interaction between PCNA and the largest subunit of RNA polymerase II, RPB1, and dissociates PCNA from actively transcribed chromatin regions, while inducing DNA double-stranded breaks in a transcription-dependent manner. Attenuation of RPB1 interaction with PCNA, by a point mutation in RPB1's PCNA-binding region, confers resistance to AOH1996. Orally administrable and metabolically stable, AOH1996 suppresses tumor growth as a monotherapy or as a combination treatment but causes no discernable side effects. Inhibitors of transcription replication conflict resolution may provide a new and unique therapeutic avenue for exploiting this cancer-selective vulnerability.

INTRODUCTION

Proliferating cell nuclear antigen (PCNA) is an evolutionarily conserved multifaceted protein found in all eukaryotic cells, and it plays a critical role in DNA synthesis and in DNA repair. PCNA forms a homo-trimeric ring structure encircling DNA¹ and it acts as a central “hub” of the replisome, to provide an anchorage for the many proteins involved in the replication and repair pathways. The cellular functions of PCNA can be modulated through post-translational modifications on the surface of the protein, altering partner interactions^{2,3} that occur predominantly through the outer hydrophobic surface of PCNA, adjacent to its inter-domain connector loop (IDCL).^{4,5} Historically, PCNA has been widely used as a tumor progression marker and more recent studies have demonstrated that PCNA can play a

mitogenic role, to distantly rejuvenate senescent cells via extracellular vesicles.⁶

DNA replication stress is a hallmark of cancer cells.^{7,8} It is used as a major anti-cancer therapeutic strategy by exploiting this cancer-associated feature, through introduction of further DNA damage resulting in catastrophic damage to the cancer cell. Due to its central role in DNA replication and repair, PCNA is a potential target for this anti-cancer strategy. Moreover, the identification of a distinct isoform of PCNA associated with cancer cells has potentially opened a novel avenue for the development of new chemotherapeutics. Early effects in targeting PCNA have identified several molecules of interest, both small molecule and peptide-based, which have indicated that directly targeting PCNA for cancer therapy may be a viable approach.^{9–15} More recent studies identified PCNA ligands, which show synergy

with existing chemotherapeutic agents.^{16–19} We previously described a compound, AOH1160,^{17,20} functioning as a potential inhibitor hit compound of the cancer-associated PCNA isoform (caPCNA), but this compound lacked suitable metabolic properties to proceed further into preclinical/clinical studies.

Here, we describe both the identification and detailed molecular characterization of AOH1996, an analog of AOH1160 that exhibits remarkable therapeutic properties: It is orally administrable in a formulation compatible with its clinical use, and in animal studies it almost completely inhibits the growth of xenograft tumors and sensitizes them to topoisomerase inhibition. In studies that follow the good laboratory practice (GLP) guidelines of the US Food and Drug Administration (FDA), AOH1996 causes no discernible toxicity at 6 or more times the effective dose in mice and dogs.

Our molecular characterizations include the structure of PCNA in complex with more soluble analogs suitable for crystallization experiments, either AOH1160-1LE or AOH1996-1LE. We showed that either of these compounds binds similarly into the PCNA-interacting protein-box (PIP-box). In cells, AOH1996 was observed to stabilize the interaction between chromatin-bound PCNA and the largest subunit (RBP1) of RNA polymerase II (RNAPII), leading to degradation of the intracellular RPB1. AOH1996 also dissociates PCNA from actively transcribed chromatin and causes DSB accumulation, without affecting the presence of PCNA in the heterochromatin region. This suggests that inhibition of caPCNA activity by AOH1996 leads to transcription-associated collapse of DNA replication. Both transcription inhibition and a point mutation within the AlkB homolog 2 PCNA interacting motif (APIM) domain²¹ of RPB1 weakens the interaction between RPB1 and PCNA; conferring resistance to AOH1996.

Transcription-replication conflicts (TRC) constitute a major intrinsic cause of DSB and genome instability.^{22,23} Given that transcription and DNA replication are essential cellular processes, and that cancer cells likely enhance encounters between the transcription and replication machineries, we suggest that this makes cancer cells more susceptible to disruption of the process leading to TRC resolution. Accumulating evidence indicates that TRC resolution involves removing RNAPII from the conflict sites, by backtracking or degradation of RNAPII. This then allows the replication fork to go through the conflict site.^{22,24} Therefore, as far as we are aware, our results are the first to demonstrate that PCNA and RBP1 interaction creates a cancer-selective vulnerability, which can be readily observed in preclinical models. Our results suggest the potential usefulness of AOH1996 as a chemical tool to further define TRCs in cells, and clearly demonstrate the therapeutic potential of AOH1996 when used as a monotherapy, as well as when it is used in combination with existing chemotherapies.

RESULTS

Targeting the PIP box and APIM binding domain of PCNA

We previously reported a small molecule PCNA ligand, AOH1160, which targets the cancer-distinct L126-Y133 region of PCNA²⁰ and is selectively toxic to cancer cells.¹⁷ By modeling the interaction between PCNA and its potential ligands using the Schrödinger suite,²⁵ we designed and synthesized approximately 70 AOH1160 analogs, in which all 3 parts of the molecule (naphthyl group, glycine linker, and diphenyl ether) were modified (see [Data S1](#) for

examples). The glycine linker was replaced with different natural and unnatural amino acids including *L*-valine, *D*-valine, *L*-alanine, *L*-lysine, *D*-lysine, *L*-glutamate, *D*-glutamate, and β -alanine. The naphthyl group was replaced with other monocyclic and bicyclic aromatic groups such as isoquinoline-1-carbonyl, isoquinoline-4-carbonyl, 2,4,6-trimethylbenzoyl, 2-(naphthalen-1-yl)acetyl, 3-(naphthalen-1-yl)propanoyl, [1,1'-biphenyl]-4-carbonyl, and 5,6,7,8-tetrahydronaphthalene-1-carbonyl ([Data S1](#) and [S2](#)). However, modifications on these two parts did not improve the AOH potency. Then, the diphenyl ether moiety was investigated for structure-activity relationship (SAR) in different ways: (1) chlorine, hydroxy, and methoxy substituents were individually introduced to the diphenyl ether group and (2) a nitrogen-walk approach was also explored on the terminal ring. This structure-activity relationship (SAR) study led to the identification of an analog, AOH1160-1LE ([Figure 1A](#)), with a predicted significant increase in solubility and AOH1996 ([Figure 1B](#)), which is derived by adding a methoxy group to the meta position of the terminal phenyl ring of AOH1160; making AOH1160-1LE more metabolically stable than AOH1160. To confirm the binding of AOH1160-1LE and AOH1996 to PCNA, we performed a thermal denaturation analysis, which is based on the principle that the binding of low molecular weight ligands can increase the thermal stability of their target proteins.²⁶ The dose-dependent protein melting curves shifted by as much as 0.5°C for AOH1160-1LE and 1.5°C for AOH1996, ([Figures 1A and 1B](#)); indicating stabilizing interactions with PCNA.

AOH1160-1LE and a more soluble AOH1996 analog, AOH1996-1LE, were both at a 4 mM concentration in an aqueous buffer with 10% DMSO, which enabled co-crystallization studies using these analogs. Using synchrotron-based data collection, we obtained a PCNA:AOH1996-1LE dataset to 3.77 Å resolution (PDB: 8GLA), and a PCNA:AOH1160-1LE co-crystal dataset to a higher 2.81 Å resolution (PDB: 8GL9) ([Table S1](#)). Phasing was provided for each structure by molecular replacement ([Table S1](#)). Four PCNA subunits are observed in the asymmetric unit of both structures, with three chains A, B, and C belonging to the homotrimeric ring structure, and the fourth chain D ([Figure 1C](#)) forming part of an adjacent ring in the unit cell that consists solely of D chains. Packing within the unit cell also places each monomer subunit of the PCNA ring against a subunit from another ring; these two stacked subunits interact via their PIP box binding pockets and IDCLs that are orientated in directly opposing directions ([Figure 1D](#)). Clearly observed within the electron density OMIT maps are three molecules of AOH1160-1LE, which bind in and adjacent to the PIP box cavity of each of the PCNA ring subunits, and these compounds have further interactions with the PIP box binding pocket of the stacked PCNA subunit ([Figure 1D](#)).

In chains A and B of the PCNA homotrimer, the central AOH1160-1LE molecule binds the PIP box binding cavity in an approximately perpendicular orientation to the binding pocket ([Figure 1E](#)). Three bound molecules are also observed in the AOH1996-1LE crystal structure ([Figure 1F](#)) and the additional methoxy group is accommodated so that the binding mode of AOH1996-1LE is comparable to that of AOH1160-1LE ([Figure 1G](#)). The central compound of AOH1160-1LE or AOH1996-1LE binds similar to what is seen with triiodothyronine (T3)¹¹ or T2 amino alcohol (T2AA) bound to PCNA²⁷ ([Figure 1H](#)). One phenyl group of the central AOH1160-1LE or AOH1996-1LE compound binds into a largely hydrophobic region of PCNA consisting of

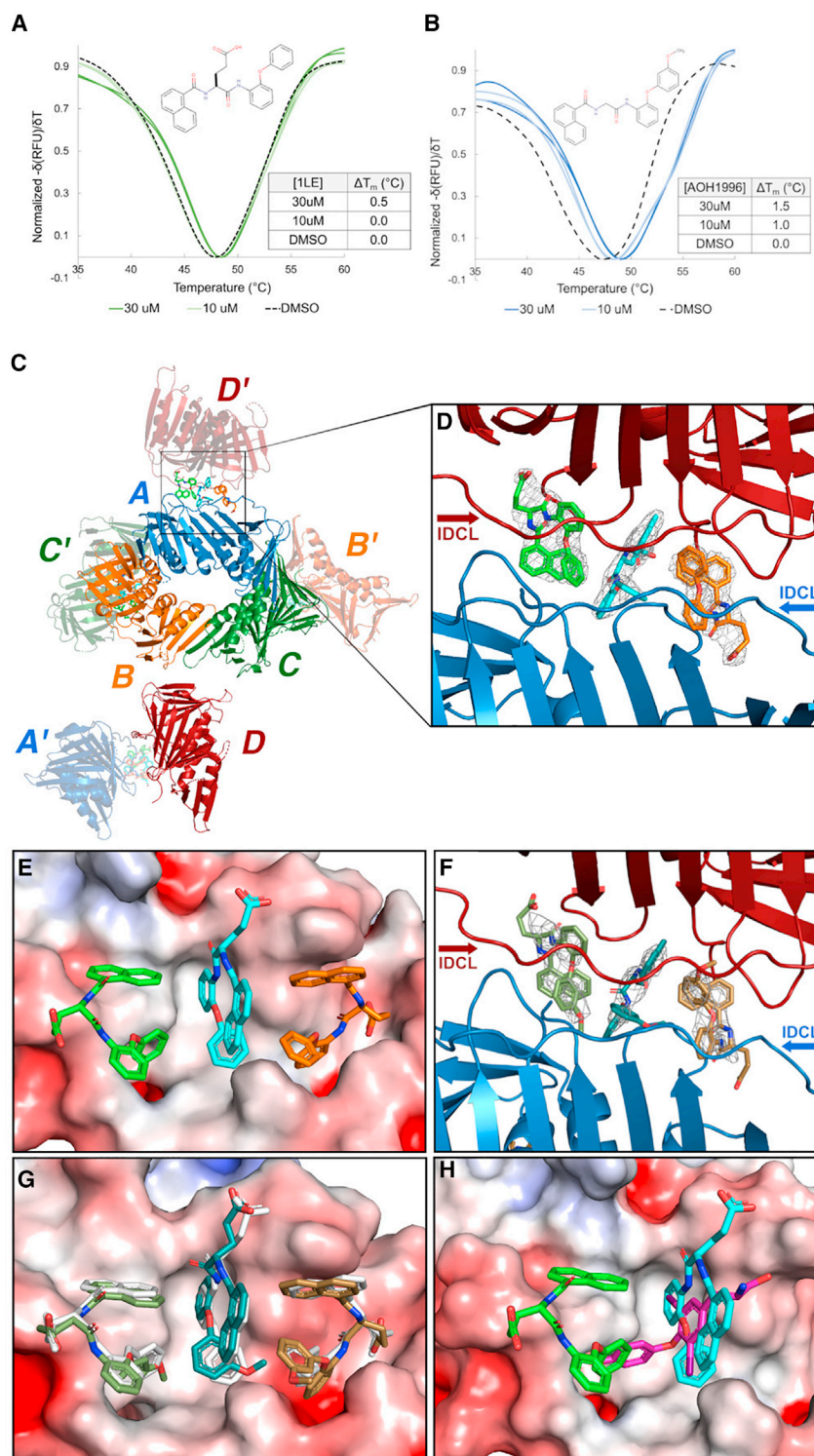


Figure 1. AOH1160 analog interactions with PCNA

(A) Thermal shift assay: Normalized inverse derivative thermal denaturation plots of 9 μ M apo-PCNA with DMSO control is depicted with a black dashed line and PCNA; in the presence of 10 μ M AOH1160-1LE is shown in light green; and 30 μ M AOH1160-1LE is shown in dark green. ΔT_m values are provided.

(B) As described in A, in the presence of 10 μ M AOH1996 is depicted in cyan and 30 μ M AOH1996 is depicted in blue.

(C) Four monomers (chains A–D) of PCNA are present in the asymmetric unit of the crystal. Chains A, B, and C form the homotrimer planar biological unit, while chain D is orientated perpendicular to, and below the plane of, the ring between chains B and C. Chain D belongs to an adjacent PCNA ring structure.

(D) Three molecules of AOH1160-1LE bind in and adjacent to the PIP box cavity of each of the PCNA ring subunits. The OMIT map, gray mesh, is contoured to 1.5 σ . Two PCNA monomer subunits from adjacent rings stack against each other, placing the PIP box and IDCLs of each subunit in opposing directions.

(E) The three AOH1160-1LE molecules, with carbon atom colored in green, cyan (central compound) and orange, are shown as stick figure representations. Two of the compounds, in green and cyan, bind into the PIP box cavity at known PCNA-partner/compound interaction sites.

(F) Three molecules of AOH1996-1LE also bind in and adjacent to the PIP box cavity of each of the PCNA ring subunits. The OMIT map, gray mesh, is contoured to 1.5 σ .

(G) Superimposition of the PCNA:AOH1160-1LE and the PCNA:AOH1996-1LE complexes, centered on the PIP box cavity, with AOH1160-1LE molecules colored in white.

(H) Superimposition of the PCNA:T2AA and the PCNA:AOH1160-1LE complexes, centered on the PIP box cavity, with T2AA carbons colored in magenta. The electrostatic surface maps are depicted with Poisson-Boltzmann electrostatic surface potentials shown in red and blue, corresponding to -5 to $+5$ kT/e respectively.

[PDB: 5MLW]⁵ [Figure S2]) and PIP box peptides (e.g., ZRANB3 PIP box peptide [PDB: 5MLO]⁵) via hydrophobic side chains. The central AOH1160-1LE or AOH1996-1LE binds in the opposite direction in the chain C and D subunits, with the naphthylene group binding to the two hydrophobic regions of the PIP box cavity (Figures S3 and S4). This is due to symmetry within the crystal, as chain C stacks against chain B', which is the symmetry mate of chain B of the ring,

while the D subunit stacks against chain A' (Figures 1C, S3, and S4). The second AOH1160-1LE or AOH1996-1LE moiety binds, via its naphthylene ring, into a region consisting of PCNA residues Val233, Pro234, Ala252, and Pro253 (Figures 1E, 1F, 1G, and S1), in addition to the compound forming a hydrogen bond to

residues His44, Val45, Leu47, Pro234, Tyr250, Leu251, and Ala252, and the second phenyl ether moiety binds into the region formed by PCNA residues Met40, Leu47, Leu126, and Ile128 (Figures 1D and S1). Multiple PIP box pocket binders also interact with these two hydrophobic regions, including T2AA and T3 via iodo groups, and APIM peptides (e.g., ZRANB3 APIM motif

while the D subunit stacks against chain A' (Figures 1C, S3, and S4). The second AOH1160-1LE or AOH1996-1LE moiety binds, via its naphthylene ring, into a region consisting of PCNA residues Val233, Pro234, Ala252, and Pro253 (Figures 1E, 1F, 1G, and S1), in addition to the compound forming a hydrogen bond to

the adjacent side chain of Asp232. This region of PCNA is bound by an aromatic group from the APIM peptide (Figure S2) and by PIP box peptides, which bind via their first aromatic side chain of the PIP box motif. One phenyl ether group of the second AOH1160-1LE or AOH1996-1LE compound binds into a pocket formed between Pro234 and Gln131, where an aromatic group of T3 and of T2AA was observed to also bind (Figures 1H and S1). Other interactions of this second compound include a potential T-shaped π -interaction between its naphthalene group and a phenyl of the diphenyl ether group of the centrally bound AOH1160-1LE or AOH1996-1LE (Figure 1G). This second compound also interacts with the stacking PCNA subunit, binding into a pocket that is immediately adjacent to the PIP box cavity of this subunit. Here, the glutamate side chain of this compound extends into this adjacent pocket to form a hydrogen bond to Ser39 of PCNA, and the remaining phenyl ether moiety binds near residues Met40, Ser42, Val123, and Leu126. The third compound bound in the PIP box cavity region binds diametrically opposite to the second: its glutamate side chain and one of the phenyl ether groups binds into the pocket that is immediately adjacent to the PIP box cavity (Figures 1G and S1). Also, the naphthalene group and second phenyl group extend into the stacking chain's PIP box pocket, to bind in the same manner as the second compound binds to its PIP box pocket. Thus, this symmetry suggests that the structure is representative of the binding of two AOH1160-1LE or AOH1996-1LE compounds, the central and second compounds as described here, which interact with residues of the PIP box cavity that are also known to be critical for the binding of PIP box and APIM peptides, and for the T2AA and T3.

To verify that AOH1160-1LE and AOH1996-1LE bound the same binding site within PCNA as was bound by AOH1996, (which is a physiologically stable analog of AOH1160 [Figure S5 and data not shown]), we created PCNA mutant cell lines using CRISPR,^{28,29} in which the leucine 47 residue (L47), (one of the amino acids contouring the compound binding pocket [Figures S1 and S4]), is substituted with a valine (Figure 2A) and tested their sensitivity to AOH1996 treatment. Compared to the wildtype parent cells, all mutant cell lines were less sensitive to growth inhibition by AOH1996; with the homozygous mutants being the least sensitive cell lines (Figure 2B). In contrast to these results with AOH1996, the L47V mutation does not apparently affect sensitivity to growth inhibition by R9-caPep (Figure 2C). R9-caPep is a cell-permeable peptide containing the L126-Y133 sequence of PCNA's IDCL region. This peptide inhibits PCNA interaction with its binding partners; presumably by acting as a "decoy" to the PIP box and APIM motif proteins,^{9,30,31} and when incubated with cancer cells, leads to cancer cell killing while having no inhibitory effect on non-cancer cell growth. These results demonstrate that the L47V mutation affects the binding of AOH1996 to PCNA without significantly changing the outer surface area of PCNA that interacts with its binding partners. Similarly, the L47V mutation confers resistance to induction of the DNA damage marker γ H2A.X by AOH1996, but not by the R9-caPep (Figure 2D). These studies support our model that AOH1996 binds to the same PCNA pocket as AOH1160-1LE.

Superior therapeutic properties of AOH1996

Based on the broad expression of AOH1996's target (caPCNA) in cancer cells²⁰ and unpublished data, we tested the compound in

more than 70 cell lines and several normal control cells. AOH1996 selectively kills cancer cells. The median concentration to achieve 50% growth inhibition (GI_{50}) was approximately 300 nM across more than 70 cancer cell lines tested (Figures S6A–S6D). In contrast, AOH1996 is not significantly toxic to nonmalignant cells, including human PBMCs, small airway epithelial cells (hSEAC), and neural crest stem cells (7SM0032), even up to a concentration of at least 10 μ M (Figures S6B and S6C). This result demonstrates no less than a 30-fold difference in sensitivity between cancer and normal cells. Consistent with these findings, AOH1996 treatment caused accumulation of DNA damages as measured by γ H2A.X levels in the SK-N-BE(2)c neuroblastoma cells (Figure S6E) and by the comet assay³² in HCC827 lung cancer cells (Figure S6F), but not in the corresponding non-malignant cells (Figures S6E and S6F). Importantly, AOH1996 is not a genotoxic mutagen. It does not cause frameshift or base pair substitution in Ames test³³ (Figure S6G).

AOH1996 induced a substantial change in cell-cycle profile that indicates G2/M and/or S phase arrest in cancer cells, but not non-malignant stem cells (Figure 3A), suggesting selective induction of replication stress in cancer cells. In addition, AOH1996 induced apoptosis as indicated by the increase in the sub-G1 population (Figure 3A) using flow cytometry and TUNEL assay positivity (Figure 3B) in cancer cells. Consistent with its lack of toxicity to nonmalignant cells (Figures S6B and S6C), AOH1996 does not significantly change the cell-cycle profiles of the nonmalignant neural crest stem cells (7SM0032) (Figure 3A) nor does it induce apoptosis in 7SM0032 cells (Figure 3B). AOH1996 increased the sensitivity of cancer cells to genotoxic agents, including cisplatin, which predominantly causes Pt-GG adducts (62–75%)³⁴ in open chromatin areas³⁵ (Figure 3C). A similar synergy profile was also observed between AOH1996 and topotecan (Figure 3D), a topoisomerase I inhibitor, which prevents topoisomerase I from re-ligating the nicked DNA strand, which subsequently causes double DNA strand breaks (DSB) during DNA replication.³⁶

One reason for synthesizing and screening AOH1160 analogs is to identify drug candidate(s) that have similar therapeutic activity but are metabolically more stable than AOH1160.¹⁷ Methoxy group on the meta position of the terminal phenyl ring of AOH1996 increases the half-life of the compound, probably due to protecting the phenyl ring from being hydroxylated by CYP enzymes.³⁷ The intended improvement in the biological stability of AOH1996 (Figure S5) would be expected to improve the pharmacokinetics (PK) of the drug and thereby improve the clinical management of patients receiving the drug. In oral PK studies using FDA-approved excipients (see STAR Methods), the compound's half-life increased by \sim 27% from 3.4 h for AOH1160 to 4.33 h for AOH1996 (Figure 4A) following an identical dose of 40 mg/kg in *ES1^e* mice.¹⁷ The improvement in half-life is accompanied by approximately a 40% increase in peak concentration (C_{max}) and nearly a 4% increase in area under the curve (AUC) (Figure 4A and 17). Comparable PK parameters of AOH1996 were observed in dog studies (Figure 4B). These studies indicate that AOH1996 is orally available to animals (with almost a 90% absorption into the circulatory system, [data not shown]) in a formulation compatible with clinical applications.

We tested the anticancer activity of AOH1996 in mice bearing xenograft tumors derived from either neuroblastoma, breast

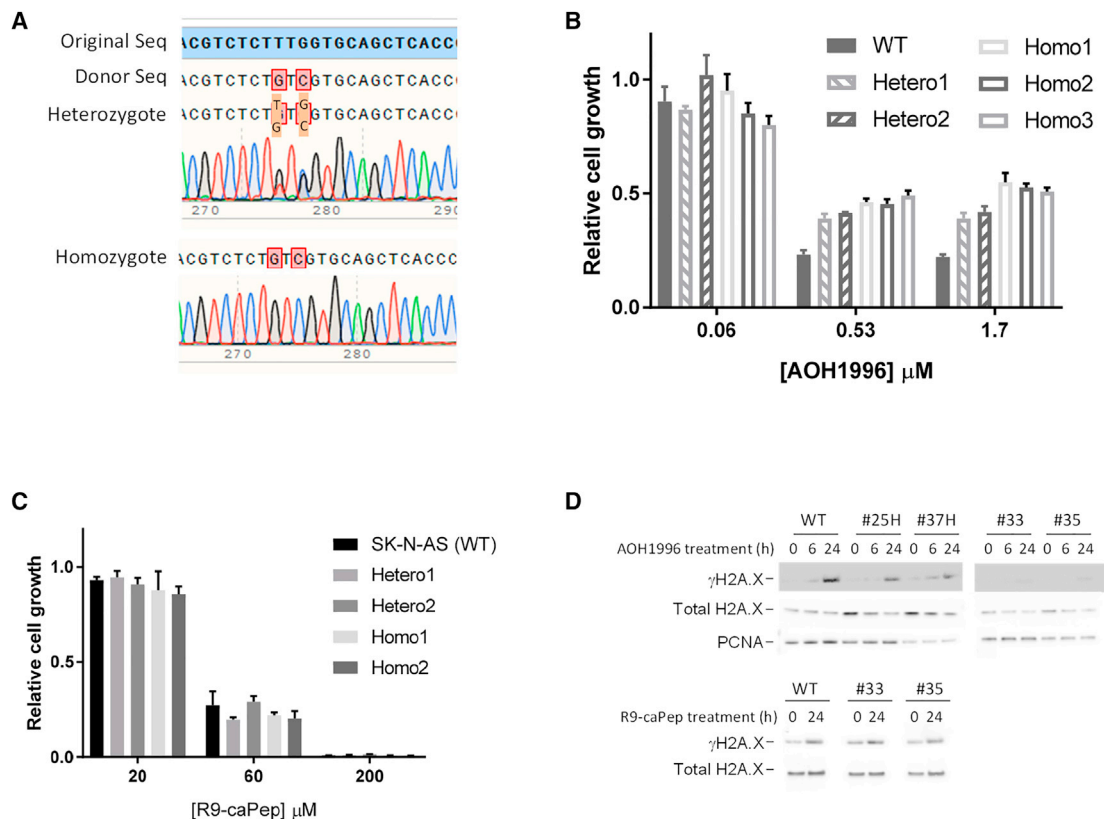


Figure 2. Interaction of AOH1996 with PCNA

(A) The PCNA gene was mutated using CRISPR, resulting in codon substitution of the Leucine 47 residue to a Valine. Shown are the DNA sequencing results of cell lines heterozygous or homozygous for the mutated gene.

(B and C) Cell lines heterozygous or homozygous for the mutated PCNA gene were treated by the indicated concentrations of AOH1996 or R9-caPep, respectively, for 72 h. The unmodified parent SK-N-AS cells were used as a control. Relative cell growth in triplicate was averaged and graphed \pm S.D.

(D) Expression of $\gamma\text{H2A.X}$ was determined by quantification of Western blots utilizing cell lines heterozygous (#25H and #37H) or homozygous (#33 and #35) for the mutated PCNA allele after cells were treated by 500 nM AOH1996 or 30 μM R9-caPep for the times indicated.

cancer, or small cell lung cancer cells (Figures 4C, 4D, and 4E, respectively). Daily AOH1996 treatment significantly reduced the tumor burden in drug-treated animals when compared to animals in the control groups that were only given vehicle in each of the tumor models (Figures 4C–4E). AOH1996 did not cause any death or significant weight loss (Figure 4F and Data S3). Furthermore, the no-observed-adverse-effect level (NOAEL) for AOH1996 was found to be ≥ 250 mg/kg/dose twice daily (BID) in mice and 75 mg/kg/dose BID in GLP-controlled toxicity studies (Not shown, filed and accepted by the US FDA). These studies consisted of 4-week chronic dosing and 2-week of post-dosing recovery periods. Based on a 3:20 dose equivalency conversion between dogs and mice (i.e., 75 mg/kg/dose in dogs is equivalent to 500 mg/kg/dose in mice),³⁸ our study demonstrated that NOAEL for AOH1996 is more than 6 times its effective dose in mouse tumor models (Figures 4C–4E).

To identify pharmacodynamics (PD) markers, we used immunohistochemistry to analyze xenograft tumors harvested from mice treated with AOH1996 or with vehicle only. Focal staining of $\gamma\text{H2A.X}$ and phospho-Chk1 was observed only in AOH1996-treated tumors (Figure 4G). Cell disintegration was often observed at or around sites showing positive staining of

$\gamma\text{H2A.X}$ and phospho-Chk1 (Figure 4G). Overall, the tumors from AOH1996-treated mice were less dense than those from the control mice. These results were consistent with the observation that AOH1996 causes DSBs (Figure 2D) and G2/M arrest (Figure 3A) in cancer cells and demonstrated the potential utility of $\gamma\text{H2A.X}$ and phospho-Chk1 as PD markers in the clinic.

We also tested the effect of AOH1996 on xenograft tumors, in combination with the topoisomerase I inhibitor CPT-11.³⁹ Tumor-bearing mice were either left untreated or were treated by AOH1996, CPT-11, or AOH1996 in combination with CPT-11. The AOH1996 treatment was given orally once daily for 8 consecutive days. Starting on the 8th day after tumor implantation, CPT-11 was given by intraperitoneal injection once daily for 3 consecutive days, and from the 12th day all animals were monitored without any further treatment until they were euthanized because of tumor overgrowth. Median survival increased by $\sim 11.5\%$. However, a single round of treatment by AOH1996 alone failed to confer a statistically significant benefit on survival, probably due to the small cohort size and the short treatment duration. Treatment with CPT-11 alone or with both AOH1996 and CPT-11 increased median survival by 34.6% and 55.4%, respectively (Figure 6H). Comparing the group treated with

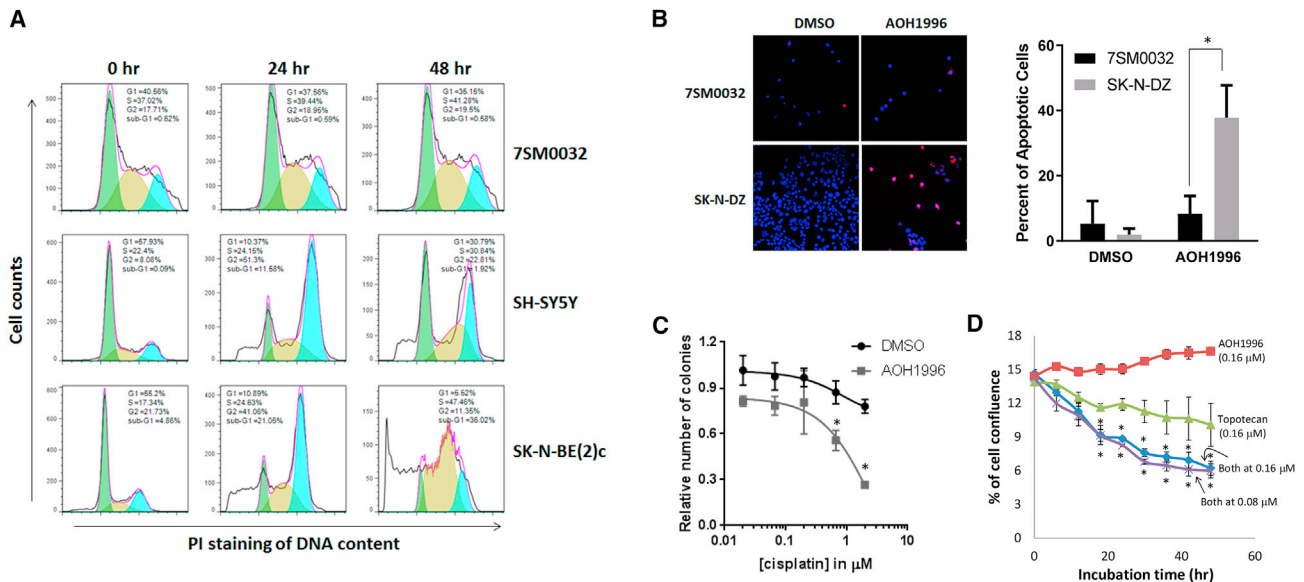


Figure 3. Therapeutic properties of AOH1996

(A) Normal neural crest stem cells (7SM0032) or cancer cells (SH-SY5Y and SK-N-BE(2)c) cells were fixed, stained with PI, and analyzed by flow cytometry following treatment with 500 nM AOH1996 for the indicated time.

(B) SK-N-DZ neuroblastoma cells and nonmalignant 7SM0032 stem cells were incubated with 500 nM AOH1996 for 24 h. Then, after being fixed on slides, cell apoptosis was analyzed by a TUNEL assay. Left: TMR fluorophore (red) attached to the free ends of DNA indicates cells undergoing apoptosis. Blue indicates DAPI stained nuclei. Right: Average abundance \pm S.D. of apoptotic 7SM0032 (black histogram) and SK-N-DZ (gray histogram) cells relative to the total number of cells are shown in 5 randomly selected fields. * $p < 0.01$.

(C) Human SK-N-DZ neuroblastoma cells were treated for 18 h with or without the indicated concentrations of cisplatin in the absence or presence of 500 nM AOH1996. Cells were washed twice with growth medium and cultured in fresh media for 18 days to allow colony formation. The colony counts in dishes treated with cisplatin but not AOH1996 (black) were normalized to the colony counts in dishes untreated by either agent. The colony counts in dishes treated by both cisplatin and AOH1996 (gray) were normalized to the colony counts in dishes treated with 500 nM AOH1996 alone. The relative number of colonies determined in triplicates for each treatment condition were averaged and graphed \pm SDs (* $p < 0.01$).

(D) SK-N-AS cells were treated with the indicated concentrations of AOH1996, topotecan, or both agents in combination. Cell growth was measured as the percentage of cell confluence by imaging every 6 h for a total of 48 h. Percent of cell confluences was averaged and graphed \pm SDs. * $p < 0.01$ in comparison with cells treated with either single agent.

AOH1996 in combination with CPT-11 with the untreated group or each of the groups treated with either agent alone, the survival benefit was statistically significant in favor of the combination treatment (Figure 4H).

Modulating PCNA's interaction with the transcription machinery

Immunoprecipitation and mass spectral analyses of PCNA interaction with its binding partners revealed that more than 50% of the proteins associated with the chromatin-bound PCNA were altered by AOH1996, and that these proteins are components of the cellular transcription process (Figure 5A). Interestingly, the only two proteins that harbor the APIM motif, (a known PCNA binding motif) identified in this mass spectral study are POLR2A (RPB1) and POL2B, both subunits of the RNAPII. Further study by immunoprecipitation discovered that AOH1996 enhanced the interaction between PCNA and RPB1 (Figure 5B) and depleted RPB1 in cancer cells (Figure 5C). In contrast, treatment with caPep, which contains the L126-Y133 sequence of PCNA that overlaps the APIM-interacting region of PCNA, blocked PCNA interaction with RPB1 (Figure 5B) and increased RPB1 levels (Figure 5C).

To determine whether the effect of AOH1996 was mediated through RPB1 interaction with PCNA, we exogenously ex-

pressed FLAG-tagged wildtype RPB1 (AMIP WT) and FLAG-tagged RPB1 in which the Y418 within the APIM motif of RPB1²¹ was replaced by an alanine (AMIP mut). Immunoprecipitation of the chromatin-bound fraction of FLAG-tagged proteins revealed that AOH1996 increased both the amount of chromatin-bound wildtype RPB1 and the amount of PCNA co-precipitated with the FLAG-tagged wildtype RPB1 (Figure 5D). This result indicated that AOH1996 increases transcription-replication conflict (TRC) and enhances interaction between RPB1 and PCNA. These effects were further enhanced by MG132, a proteasome inhibitor, suggesting that AOH1996 can induce RPB1 proteasomal degradation, possibly by modulating RPB1 interaction with PCNA. In contrast, co-precipitation of PCNA with the FLAG-tagged AMIP mut RPB1 was only detectable at a reduced level in the presence of AOH1996 and MG132 (Figure 5D); indicating a weakened interaction between PCNA and the RPB1 containing the Y418 mutation; which is partially compensated by the presence of AOH1996 and MG132. Examining the level of exogenously expressed RPB1 in whole cell extracts, we found that AOH1996 caused degradation of the wildtype RPB1, but not the APIM mut form, in a proteasome-dependent manner (Figure 5E). Interestingly, the APIM mut RPB1 was as susceptible to UV-induced degradation as the wildtype RPB1; indicating that the mutant RPB1 selectively confers resistance to

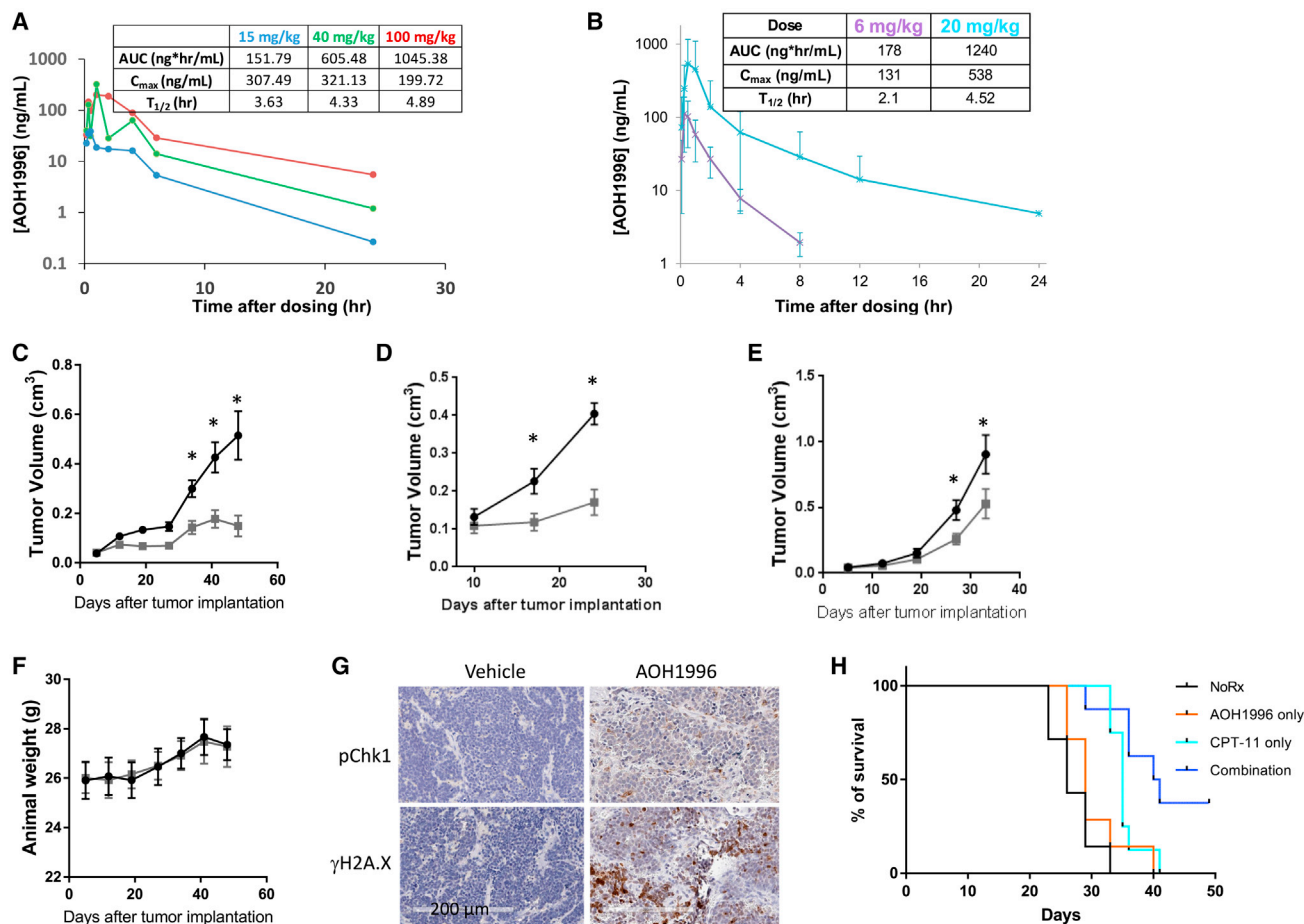


Figure 4. Pharmacokinetics and anti-tumor growth activity of AOH1996 *in vivo*

(A) After oral administration, the plasma concentrations of AOH1996 from three male and three female ES1^o/SCID mice at the indicated time points were averaged and graphed \pm S.D. The inset contains PK parameters determined by a standard non-compartmental method.

(B) A similar PK study of AOH1996 was performed in dogs.

(C–E) ES1^o/SCID mice bearing the xenograft tumors of neuroblastoma (C: SK-N-BE(2)c), breast cancer (D: MDA-MB-468), and small-cell lung cancer (E: H82) were given vehicle only (black) or 40 mg/kg of AOH1996 (gray) twice daily immediately after the first measurement. Tumor sizes were measured by a dial caliper each week. Tumor volumes ($0.4 \times L \times W^2$) were averaged and graphed \pm S.E. (*, $p < 0.01$).

(F) Animal body weight was monitored throughout the studies as an indicator of toxicity. Shown are typical study results (average \pm S.E.) from the study of the SK-N-BE(2)c tumor model described in (C).

(G) The levels of phosphor-Chk1 (pChk1) and γ H2A.X in SK-N-BE(2)c derived tumor samples were analyzed by IHC. Shown are representative images taken from tumors treated by vehicle only or by 40 mg/kg AOH1996.

(H) ES1^o/SCID mice bearing SK-N-AS derived xenograft tumors were treated with either 80 mg/kg of AOH1996 (black, $n = 7$) for 8 days beginning 8 days after tumor implantation, 15 mg/kg of CPT-11 ($n = 8$) for 3 days beginning 12 days after tumor implantation, or both agents (combination, $n = 8$) under the same dosages and schedules as they were dosed alone. Mice implanted with the same tumor and left untreated were used as control ($n = 8$). Shown are the survival graphs. The p values determined by the Log rank (Mantel-Cox) test between combination treatment and each of the control groups are $p = 0.0003$ (Combination vs. NoRx), $p = 0.005$ (Combination vs. AOH1996 alone), and $p = 0.024$ (Combination vs. CPT-11 alone).

degradation triggered possibly by stalled transcription mediated by replisomal conflict with the transcription machinery, but not by UV-created DNA lesion.

We mutated Y418 of RPB1 to an alanine in the SK-N-AS cell line using CRISPR. Cells homozygous of the Y418A mutant alleles were significantly less sensitive to growth inhibition by AOH1996 than the parent cells (Figure 6A). Mass spectral and gene ontology (GO) enrichment analyses showed that proteins involved in cell cycle regulation and DNA replication and repair represent 49 out of 54 unique proteins whose levels were changed at least 2-fold by AOH1996 treatment

in either cell line, with a p value less than 0.05 (Figure 6B). Most of the changes caused by AOH1996 treatment are much higher in the parent cells than in the RBP1 mutant cells (Figure 6C), again indicating that AOH1996 exerts its effects, at least partially, through modulating PCNA interaction with RPB1.

Transcription dependent dissociation of PCNA from chromatin

To determine the effect of altered PCNA and RBP1 interaction on DNA replication, we treated the chromatin pellet with RNase A to

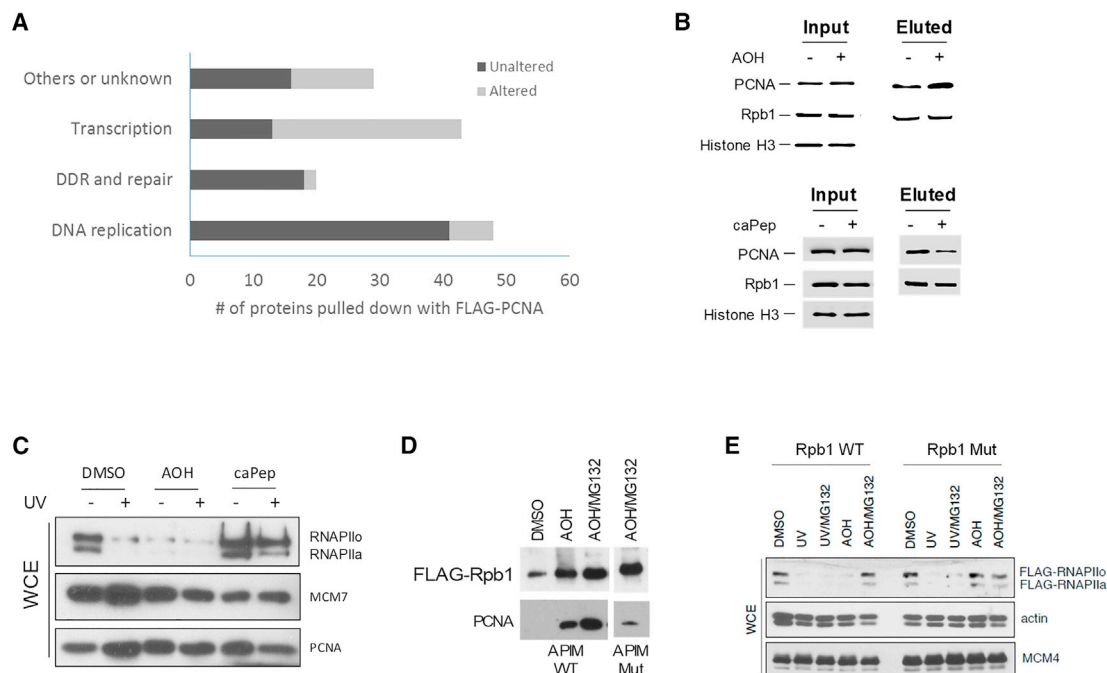


Figure 5. Modulation of PCNA interaction with RNA polymerase II

(A) Chromatin-bound (CB) proteins were fractionated from HEK293T cells expressing FLAG-tagged PCNA after the cells were treated with or without 500 nM AOH1996. Proteins in complex with FLAG-PCNA were immune-precipitated and analyzed by mass spectrometry. Shown are numbers of proteins whose abundances were unaltered (black) or altered (gray) by more than 2-fold following AOH1996 treatment.

(B) SK-N-AS cells exogenously expressing an FLAG-tagged RPB1 gene were fractionated prior to, and after, being treated overnight with 500 nM AOH1996. PCNA in complex with chromatin-bound (CB) FLAG-RBP1 was analyzed by Western blotting.

(C) Human SK-N-AS cells were treated with UV in the presence or absence of AOH1996 (AOH) or R9-caPep (caPep). Whole cell extracts were analyzed by Western blotting.

(D) Cells exogenously expressing FLAG-tagged wildtype RPB1 or FLAG-tagged APIM-mutant RPB1 gene were fractionated. PCNA in complex with chromatin-bound (CB) FLAG-RBP1 was analyzed by Western blotting.

(E) HEK293T cells were transiently transfected with an FLAG-tagged wildtype RPB1 (APIM WT) gene or mutant RPB1 gene (APIM mutant). The intracellular MCM7 and RBP1 (both the hypo-phosphorylated RNAPII α and hyper-phosphorylated RNAPII β forms) was analyzed by Western blotting after cells were treated by the indicated agents and/or UV.

destabilize the open chromatin structures^{40,41} and to solubilize active transcription factors, chromatin remodeling enzymes, and DNA replication factors from open chromatin.⁴² After the solubilized fraction (CB:RNA+, Figure 7A) was removed, the remaining insoluble pellet was further digested with benzonase to produce the protein fraction (CB:RNA-, Figure 7A) enriched for the heterochromatin marker of CAF-1.²⁴ Interestingly, AOH1996 caused dissociation of PCNA and MCM7 from the actively transcribed open chromatin regions (Figure 7A) but did not cause much change in their presence at low or non-transcribed heterochromatin regions (Figure 7A). This result suggested that AOH1996 causes collapse of DNA replication forks but only in the presence of active transcription.

To measure the effect of AOH1996 on DNA replication fork extension directly, we pulsed synchronized S phase cells with a modified thymidine analog (CldU) in the absence of AOH1996. After washing away the unincorporated CldU, we incubated cells with a second thymidine analog (IdU) in the presence or absence of AOH1996. The DNA replication fork extension before and after AOH1996 treatment was quantified by measuring the relative length of CldU-incorporated DNA strands and adjacent IdU-incorporated DNA strands, respec-

tively. Before AOH1996 treatment, the average lengths of the CldU-incorporated DNA strands (Figure 7B, green strands or bars) were similar between the control and experimental cells, indicating similar DNA replication forks extension. In contrast, the IdU-incorporated DNA strands became significantly shorter in cells treated with AOH1996 than in untreated control cells (Figure 7B, red strands and bars) indicating interference with DNA replication.

Consistent with our mechanistic model that AOH1996 exerts its effect by modulating PCNA interaction with RPB1, AOH1996 treatment caused substantially more DNA damage as measured by γ H2A.X levels in cells containing the wildtype RPB1 allele than in cells homozygous of the Y418A mutant allele (Figure 7C). The transcription inhibitor DRB suppresses the DNA damage induced by AOH1996 (Figure 7D), which confirms that the effect of the compound on DNA damage is transcription dependent. Consistent with TRC induction, AOH1996 treatment causes accumulation of R-loops, a three-stranded nucleic acid structure consisting of a DNA:RNA hybrid (Figure 7E). Overexpression of RNase H1 can reduce R-loop levels (Figure 7E) and DNA damage (Figure 7F) induced by AOH1996, indicating that AOH1996 causes DNA

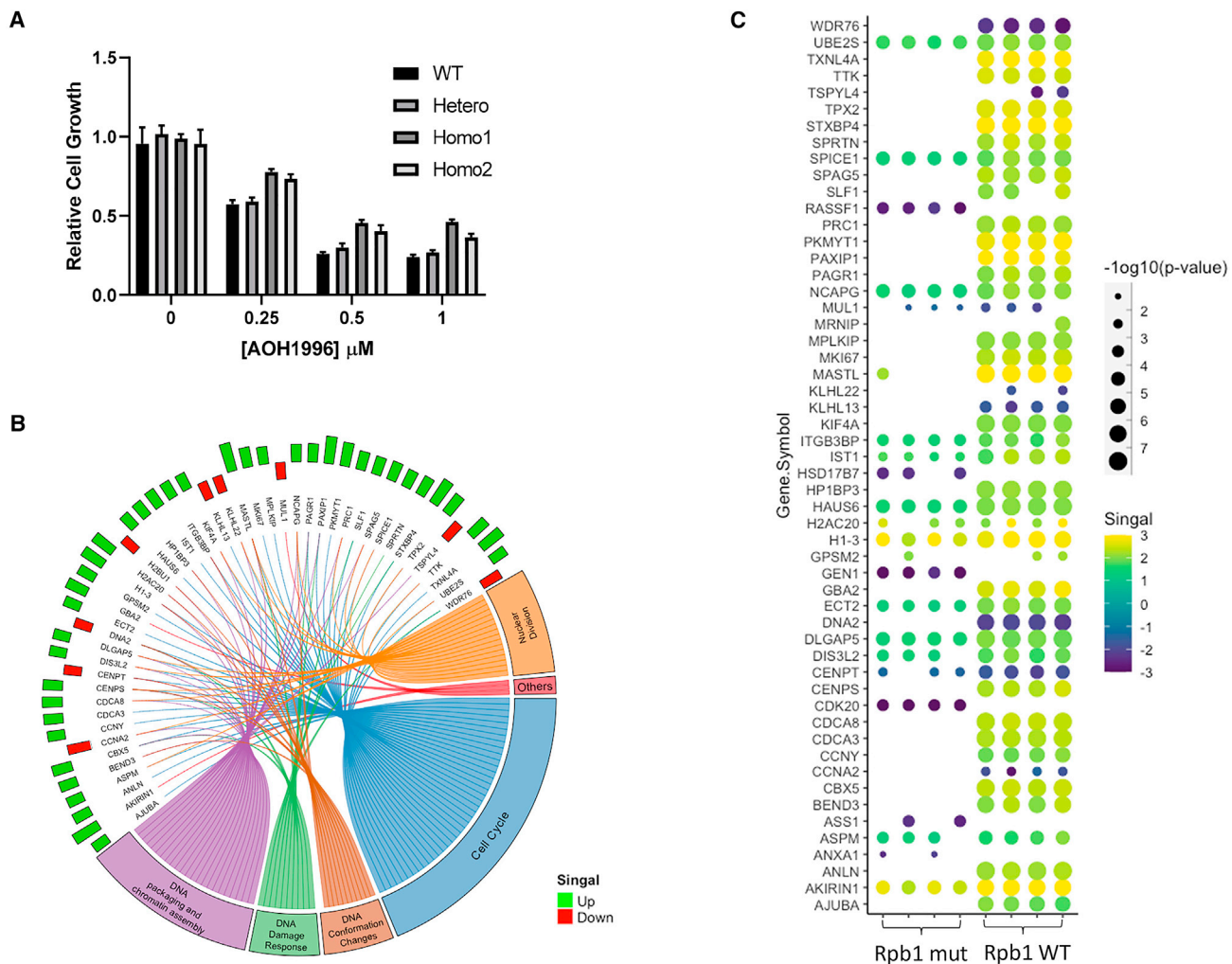


Figure 6. The effect of AOH1996 is mediated through PCNA interaction with RPB1

(A) Cell lines heterozygous or homozygous for the APIM-mutant RPB1 gene were treated for 72 h with the indicated concentrations of AOH1996. The parent SK-N-AS cells were used as control. Relative cell growth in triplicate was averaged and graphed \pm S.D.

(B) Whole cell proteome from SK-N-AS cells homozygous for the APIM-mutant RPB1 gene was analyzed by mass spectrometry before and after the cells were treated overnight in quadruplicate with 500 nM AOH1996. To average out any clonal differences unrelated to the RPB1 mutation, the quadruplicated samples were derived from 2 independent RPB1 mutant clones. The unmodified parent SK-N-AS cells in quadruplicates were used as the control. The enrichment of proteins in cells of either genotype, whose expression was altered by AOH1996 treatment by at least 2-fold, and exhibited a p value less than 0.05, was analyzed by MetaCore's gene ontology program, (Clarivate Analytics, Philadelphia, PA). Shown in the Cricos diagram are the enriched GO processes these proteins associated with and the average fold change of their expression induced by AOH1996 treatment.

(C) The fold change in the expression of the proteins identified in B was calculated for each AOH1996-treated sample, relative to the average expression level in the corresponding untreated cells and then visualized in the dot plot heatmap. Also shown in the dot plot heatmap is the statistical significance expressed in $-\log_{10}(p\text{ value})$ between treated and untreated samples of the same genotype.

damage at least partially through inducing R-loop formation in cancer cells.

DISCUSSION

Besides oncogenes, the survival of cancer cells depends on several stress response pathways including those for oxidative damage, DNA damage, and heat shock, all of which play critical roles in normal and ubiquitous cellular functions.⁴³ While not oncogenic themselves, many of the rate-limiting proteins in these pathways are essential for dealing with the increased

stresses in cancer cells.⁴³ Increasingly, cancer drug discovery has targeted these non-oncogenic pathways, and efforts have yielded a number of successful therapeutics (see⁴⁴ for review). Unlike oncogenes, target genes in these non-oncogenic pathways do not undergo oncogenic mutations or functionally significant genomic alterations in tumors. Therefore, they represent points of intervention less prone to the development of resistance. Acting as a central "hub" in the DNA replication/repair pathways, and interacting with many other cellular pathways, including mRNA transcription, PCNA is one of the non-oncogene proteins essential for the growth and survival of cancer cells.

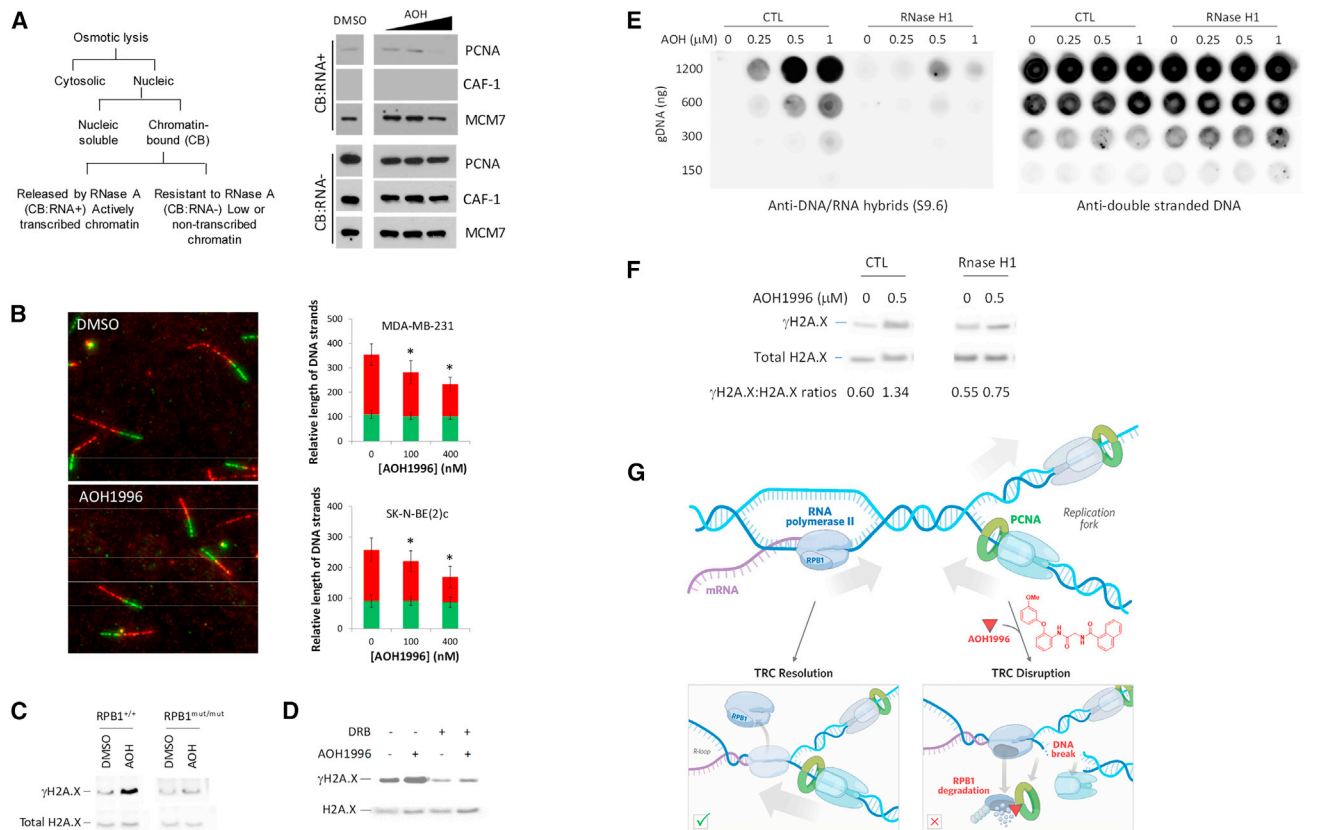


Figure 7. Transcription dependent effect on DNA replication and damage

(A) Left: Schematic of the cell fractionation procedure. Right: MDA-MB-468 cells were treated with increasing concentrations of AOH1996 (5, 50, or 500 nM) for 24 h. Cells treated with only the equivalent concentration of DMSO were used as the control. Whole cell extract (WCE) and protein fractions associated with actively transcribed chromatin (CB:RNA+) or with low or non-transcribed chromatin (CB:RNA-) were analyzed by Western blot using antibodies against PCNA, CAF-1, and MCM7.

(B) Synchronized cancer cells by serum starvation were sequentially incubated in the presence of CldU (green) and IdU (red) before and after AOH1996 treatment, respectively. Cells sequentially incubated with the same two nucleotide analogs but without AOH1996 were used as the control. Left: Representative images of labeled DNA strands from untreated cells or cells treated with AOH1996. Middle and Right: Lengths of CldU (green) and IdU (red) incorporated DNA segments measured for more than 30 independent DNA strands from the indicated cancer cell type were averaged and graphed \pm S.D. * $p < 0.01$ in comparison with the corresponding samples untreated by AOH1996.

(C) Whole cell lysates were extracted from SK-N-AS cells homozygous for the wildtype RPB1 allele or the APIM-mutant allele. Histone H2A.X and γ H2A.X was analyzed by Western blot following overnight incubation with AOH1996 in DMSO or with just DMSO, which served as the control. t.

(D) Histone H2A.X and γ H2A.X in whole cell lysates from SK-N-AS cells were analyzed by Western blot after treatment with 500 nM AOH1996 and/or 50 μ M DRB overnight.

(E) SK-N-AS cells were transiently transfected with a plasmid expressing the human RNase H1 gene. Cells transfected with an empty vector were used as control (CTL). Left panel: R-loop levels in genomic DNAs extracted from cells treated by AOH1996 at the indicated concentration were analyzed by dot blotting with S9.6 antibody, Right panel: Double-stranded DNA levels of the same samples were measured by an antibody specific to double-stranded DNAs.

(F) The histone H2A.X and γ H2A.X levels in SK-N-AS cells transiently transfected by the RNase H1 expression plasmid or an empty vector were measured by Western blot before and 24 h after AOH1996 treatment.

(G) A working model of the mechanism of action of AOH1996: binding of AOH1996 to PCNA stabilizes PCNA interaction with RNA polymerase II and interferes with TRC resolution leading to dissociation of PCNA from chromatin in a transcription dependent manner. By exploiting this cancer vulnerability, AOH1996 selectively inhibits tumor growth without causing any discernible side effect.

Our study reports two new AOH1160-based inhibitor analogs, with the readily soluble analogs AOH1160-1LE and AOH1996-1LE that clearly demonstrate binding to the PCNA PIP Box binding cavity. The second is a cell-permeable and more metabolically stable compound, AOH1996, which is a lead compound with drug-like characteristics.

Our studies reveal that AOH1996 enhances the interaction between PCNA and RPB1. This leads to the overall degradation of

RPB1 and collapse of DNA replication forks in actively transcribed chromatin regions. The transcription and replication processes are both highly active in fast-growing cancer cells. Firing of dominant replication origins driven by oncogenes further dysregulates the spatiotemporal segregation of transcription and replication during the S-phase in cancer cells.⁴⁵ Thus, resolving TRC is paramount to the growth and survival of cancer cells, as the level of replication stress TRC causes can lead to genome

instability and lethal DNA damage. Yet, the mechanisms to resolve TRC have yet to be fully elucidated, and TRC has not been examined as a viable therapeutic target.

Based on our findings, we now propose a working model to target TRC (Figure 7G). When the transcription and replication machineries encounter each other on a chromosome, the RNA polymerase is temporarily removed from the collision site, leaving the unfinished RNA transcript forming an R-loop structure with the DNA template. It has been shown that PCNA plays a role in the process of dislodging RNA polymerase.²⁴ In this report we demonstrate that RPB1 interacts with PCNA through its APIM motif, possibly by interacting with the outer hydrophobic surface adjacent to the inter-domain connector loop (IDCL) of PCNA, which interacts with AOH1996. The binding of AOH1996 to PCNA likely stabilizes the disordered IDCL region, as per the AOH1160-1LE and AOH1996-1LE crystal structures, and, as noted in other PCNA co-complex structures,⁴⁶ it likely enhances the interaction of PCNA with RPB1. This interaction thereby prevents the displacement of RNA polymerase and TRC resolution, which results in the persistent presence of unresolved TRC. This in turn leads to the lethal DSB but also disrupts the transcription machinery by causing RPB1 degradation.

Overall, the presence of the cancer-associated isoform of PCNA disrupts the PCNA-TRC interface in cancer cells and enables AOH1996 to exert potent, selective anticancer effects, while maintaining a remarkable clinical safety profile. Thus, our study highlights the utility of AOH1996 as a research tool to aid in the molecular characterization of the TRC process in cancer cells and demonstrates this lead compound's therapeutic potential.

Limitations of the study: We demonstrated a unique mechanism by which AOH1996 binds to PCNA and stabilizes the interaction between PCNA and RPB1, thereby interfering with the resolution of transcription-replication conflicts. Given the multifunctionality of PCNA, this action mechanism is unlikely the only way by which AOH1996 exerts its anti-cancer activity. Further studies of this compound on other aspects of PCNA functions will be needed to fully define its action mechanism. This study reports the anti-cancer activity of AOH1996 in a broad range of cancer cells and several animal tumor models. We acknowledge that positive animal study results do not always translate into success in treating cancer patients. Future clinical studies are necessary to determine its efficacy for cancer treatment.

SIGNIFICANCE

A key hallmark of a cancer cell is replication stress and genome instability, and some of the leading chemotherapies exploit this hallmark, by introducing further DNA damage that results in catastrophic consequences for the cancer cell. The high incidence of transcription replication conflicts (TRC) is a major contributor to genomic instability within cancer cells, and TRCs likely provide a potential, but not yet utilized target for chemotherapy development. Directly testing this hypothesis of targeting TRC for selective killing cancer cells has been difficult, largely due to a lack of small molecule tools that can target the resolution of TRC. Here, we report a small molecule inhibitor, AOH1996, of a cancer-associated isoform of PCNA (caPCNA), which notably, almost completely inhibits the growth of xenograft tumors without causing any

discernible toxicity to experimental animals. Mechanistically, AOH1996 stabilizes the interaction between chromatin-bound PCNA and the largest subunit (RPB1) of RNA polymerase II (RNAPII) and leads to degradation of the intracellular RPB1. AOH1996 selectively dissociates PCNA from actively transcribed chromatin and causes DSB accumulation in a transcription-dependent manner, without affecting the presence of PCNA in the heterochromatin region. This indicates that inhibition of caPCNA activity by AOH1996 leads to transcription-associated collapse of DNA replication. Taken together, our studies have characterized the unique molecular mechanisms of this now investigational new drug, which has entered Phase 1 clinical trials, and they have validated the drug's unique mechanism of action by which inhibition of transcription-replication conflict resolution likely opens a new therapeutic avenue for the selective killing of cancer cells.

STAR★METHODS

Detailed methods are provided in the online version of this paper and include the following:

- KEY RESOURCES TABLE
- RESOURCE AVAILABILITY
 - Lead contact
 - Materials availability
 - Data and code availability
- EXPERIMENTAL MODEL AND STUDY PARTICIPANT DETAILS
 - Plasmids and cell lines
 - Animals
- METHODS DETAILS
 - Computer modeling
 - Transfection
 - Purification and crystallization of PCNA
 - Thermal denaturation assay for PCNA-AOH1996 interaction
 - Crystallization and X-ray data analysis
 - Establishment of mutant cell lines by CRISPR
 - Cell cycle analysis
 - Cell growth and apoptosis assays
 - DNA combing analysis
 - Clonogenic assay
 - Western and dot blot
 - Cell fractionation and immunoprecipitation
 - Compound metabolism in liver microsome
 - Proteomic analysis using mass spectrometry
 - Pharmacokinetic (PK) study in animals
 - *In vivo* tumor model
- QUANTIFICATION AND STATISTICAL ANALYSIS

SUPPLEMENTAL INFORMATION

Supplemental information can be found online at <https://doi.org/10.1016/j.chembiol.2023.07.001>.

ACKNOWLEDGMENTS

The authors thank Dr. Steven L. Vonderfecht for his assistance in carrying out the toxicology study. This work was supported in part by research awards to

LHM from the Department of Defense (W81XWH-11-1-0786), National Institutes of Health/National Cancer Institute (R01 CA121289), St Baldrick's Foundation (www.stbaldricks.org), the Alex's Lemonade Stand Foundation for Childhood Cancer (Rich Award), Tobacco-Related Disease Research Program (TRDRP-T31IP626), Melanoma Research Foundation (MRF-717178), and the ANNA Fund (www.annafund.com), to Y.L. from National Institutes of Health/National Cancer Institute (R01 CA225843), to K.S.A. from the Raikes Foundation, to R.J.H. and J.J.P.P. from CDMRP of the Department of Defense (W81XWH-19-1-0326 under BC181474 and BC181474P1, respectively). In addition, research reported in this publication was supported by the Analytical Pharmacology Core supported by the National Cancer Institute of the National Institutes of Health under grant number P30CA033572. The content is solely the responsibility of the authors and does not necessarily represent the official views of the National Institutes of Health or the Congressionally Directed Medical Research Programs. The funders had no role in study design, data collection and analysis, decision to publish, or preparation of the manuscript.

AUTHOR CONTRIBUTIONS

L.H.M., R.J.H., Y.L., V.C., D.V.H., K.S.A., J.J.P.P., and L.G. conceptualized the idea and supervised the project; L.G., M.L., R.L., J.J., and C.M.L. designed and performed most experiments; T.W.S. designed and supervised the pharmacokinetics studies; D.H. and P.H. were responsible for the design and synthesis of the analog compounds; M.G., L.F., and C.H. performed the *in vivo* combination therapy study; J.J. primarily performed the crystallography studies with support from N.K.; H.L. performed the computer modeling analysis; B.L. performed the proteomic study; H.L. analyzed the proteomic data; L.G. and J.J.P.P. wrote the manuscript.

DECLARATION OF INTERESTS

The authors declare the following competing financial interest(s): City of Hope's Office of Technology Licensing has been awarded a patent on AOH1996 and its analogs. L.H. Malkas, R.J. Hickey, D. Horne, and L. Gu are listed as inventors.

Received: May 12, 2022

Revised: February 12, 2023

Accepted: July 10, 2023

Published: August 1, 2023

REFERENCES

1. Krishna, T.S., Kong, X.P., Gary, S., Burgers, P.M., and Kuriyan, J. (1994). Crystal structure of the eukaryotic DNA polymerase processivity factor PCNA. *Cell* 79, 1233–1243.
2. Tsutakawa, S.E., Van Wynsberghe, A.W., Freudenthal, B.D., Weinacht, C.P., Gakhar, L., Washington, M.T., Zhuang, Z., Tainer, J.A., and Ivanov, I. (2011). Solution X-ray scattering combined with computational modeling reveals multiple conformations of covalently bound ubiquitin on PCNA. *Proc. Natl. Acad. Sci. USA* 108, 17672–17677.
3. Tsutakawa, S.E., Yan, C., Xu, X., Weinacht, C.P., Freudenthal, B.D., Yang, K., Zhuang, Z., Washington, M.T., Tainer, J.A., and Ivanov, I. (2015). Structurally distinct ubiquitin- and sumo-modified PCNA: implications for their distinct roles in the DNA damage response. *Structure* 23, 724–733.
4. Chapados, B.R., Hosfield, D.J., Han, S., Qiu, J., Yelent, B., Shen, B., and Tainer, J.A. (2004). Structural basis for FEN-1 substrate specificity and PCNA-mediated activation in DNA replication and repair. *Cell* 116, 39–50.
5. Sebesta, M., Cooper, C.D.O., Ariza, A., Carnie, C.J., and Ahel, D. (2017). Structural insights into the function of ZRANB3 in replication stress response. *Nat. Commun.* 8, 15847.
6. Lei, Q., Gao, F., Liu, T., Ren, W., Chen, L., Cao, Y., Chen, W., Guo, S., Zhang, Q., Chen, W., et al. (2021). Extracellular vesicles deposit PCNA to rejuvenate aged bone marrow-derived mesenchymal stem cells and slow age-related degeneration. *Sci. Transl. Med.* 13, eaaz8697.
7. Hanahan, D., and Weinberg, R.A. (2011). Hallmarks of cancer: the next generation. *Cell* 144, 646–674.
8. Hanahan, D., and Weinberg, R.A. (2000). The hallmarks of cancer. *Cell* 100, 57–70.
9. Gu, L., Smith, S., Li, C., Hickey, R.J., Stark, J.M., Fields, G.B., Lang, W.H., Sandoval, J.A., and Malkas, L.H. (2014). A PCNA-derived cell permeable peptide selectively inhibits neuroblastoma cell growth. *PLoS One* 9, e94773.
10. Müller, R., Misund, K., Holien, T., Bachke, S., Gilljam, K.M., Våtsveen, T.K., Rø, T.B., Bellacchio, E., Sundan, A., and Otterlei, M. (2013). Targeting proliferating cell nuclear antigen and its protein interactions induces apoptosis in multiple myeloma cells. *PLoS One* 8, e70430.
11. Punchihewa, C., Inoue, A., Hishiki, A., Fujikawa, Y., Connelly, M., Evison, B., Shao, Y., Heath, R., Kuraoka, I., Rodrigues, P., et al. (2012). Identification of small molecule proliferating cell nuclear antigen (PCNA) inhibitor that disrupts interactions with PIP-box proteins and inhibits DNA replication. *J. Biol. Chem.* 287, 14289–14300.
12. Tan, Z., Wortman, M., Dillehay, K.L., Seibel, W.L., Evelyn, C.R., Smith, S.J., Malkas, L.H., Zheng, Y., Lu, S., and Dong, Z. (2012). Small-molecule targeting of proliferating cell nuclear antigen chromatin association inhibits tumor cell growth. *Mol. Pharmacol.* 81, 811–819.
13. Waga, S., Hannon, G.J., Beach, D., and Stillman, B. (1994). The p21 inhibitor of cyclin-dependent kinases controls DNA replication by interaction with PCNA. *Nature* 369, 574–578.
14. Yu, Y.L., Chou, R.H., Liang, J.H., Chang, W.J., Su, K.J., Tseng, Y.J., Huang, W.C., Wang, S.C., and Hung, M.C. (2013). Targeting the EGFR/PCNA signaling suppresses tumor growth of triple-negative breast cancer cells with cell-penetrating PCNA peptides. *PLoS One* 8, e61362.
15. Zhao, H., Lo, Y.H., Ma, L., Waltz, S.E., Gray, J.K., Hung, M.C., and Wang, S.C. (2011). Targeting tyrosine phosphorylation of PCNA inhibits prostate cancer growth. *Mol. Cancer Therapeut.* 10, 29–36.
16. Lu, S., and Dong, Z. (2019). Additive effects of a small molecular PCNA inhibitor PCNA-I1S and DNA damaging agents on growth inhibition and DNA damage in prostate and lung cancer cells. *PLoS One* 14, e0223894.
17. Gu, L., Lingeman, R., Yakushijin, F., Sun, E., Cui, Q., Chao, J., Hu, W., Li, H., Hickey, R.J., Stark, J.M., et al. (2018). The Anticancer Activity of a First-in-class Small-molecule Targeting PCNA. *Clin. Cancer Res.* 24, 6053–6065.
18. Dillehay, K.L., Lu, S., and Dong, Z. (2014). Antitumor effects of a novel small molecule targeting PCNA chromatin association in prostate cancer. *Mol. Cancer Therapeut.* 13, 2817–2826.
19. Bartolowits, M.D., Gast, J.M., Hasler, A.J., Cirrincione, A.M., O'Connor, R.J., Mahmoud, A.H., Lill, M.A., and Davisson, V.J. (2019). Discovery of Inhibitors for Proliferating Cell Nuclear Antigen Using a Computational-Based Linked-Multiple-Fragment Screen. *ACS Omega* 4, 15181–15196.
20. Malkas, L.H., Herbert, B.S., Abdel-Aziz, W., Dobrolecki, L.E., Liu, Y., Agarwal, B., Hoelz, D., Badve, S., Schnaper, L., Arnold, R.J., et al. (2006). A cancer-associated PCNA expressed in breast cancer has implications as a potential biomarker. *Proc. Natl. Acad. Sci. USA* 103, 19472–19477.
21. Gilljam, K.M., Feyzi, E., Aas, P.A., Sousa, M.M.L., Müller, R., Vågbo, C.B., Catterall, T.C., Liabakk, N.B., Slupphaug, G., Drablos, F., et al. (2009). Identification of a novel, widespread, and functionally important PCNA-binding motif. *J. Cell Biol.* 186, 645–654.
22. Helmrich, A., Ballarino, M., Nudler, E., and Tora, L. (2013). Transcription-replication encounters, consequences and genomic instability. *Nat. Struct. Mol. Biol.* 20, 412–418.
23. Gaillard, H., and Aguilera, A. (2016). Transcription as a Threat to Genome Integrity. *Annu. Rev. Biochem.* 85, 291–317.
24. Li, M., Xu, X., Chang, C.W., Zheng, L., Shen, B., and Liu, Y. (2018). SUMO2 conjugation of PCNA facilitates chromatin remodeling to resolve transcription-replication conflicts. *Nat. Commun.* 9, 2706.
25. Friesner, R.A., Murphy, R.B., Repasky, M.P., Frye, L.L., Greenwood, J.R., Halgren, T.A., Sanschagrin, P.C., and Mainz, D.T. (2006). Extra precision

- glide: docking and scoring incorporating a model of hydrophobic enclosure for protein-ligand complexes. *J. Med. Chem.* **49**, 6177–6196.
26. Koshland, D.E. (1958). Application of a Theory of Enzyme Specificity to Protein Synthesis. *Proc. Natl. Acad. Sci. USA* **44**, 98–104.
 27. Inoue, A., Kikuchi, S., Hishiki, A., Shao, Y., Heath, R., Evison, B.J., Actis, M., Canman, C.E., Hashimoto, H., and Fujii, N. (2014). A small molecule inhibitor of monoubiquitinated Proliferating Cell Nuclear Antigen (PCNA) inhibits repair of interstrand DNA cross-link, enhances DNA double strand break, and sensitizes cancer cells to cisplatin. *J. Biol. Chem.* **289**, 7109–7120.
 28. de la Fuente-Núñez, C., and Lu, T.K. (2017). CRISPR-Cas9 technology: applications in genome engineering, development of sequence-specific antimicrobials, and future prospects. *Integr. Biol.* **9**, 109–122.
 29. Hsu, P.D., Lander, E.S., and Zhang, F. (2014). Development and applications of CRISPR-Cas9 for genome engineering. *Cell* **157**, 1262–1278.
 30. Gu, L., Chu, P., Lingeman, R., McDaniel, H., Kechichian, S., Hickey, R.J., Liu, Z., Yuan, Y.C., Sandoval, J.A., Fields, G.B., and Malkas, L.H. (2015). The Mechanism by Which MYCN Amplification Confers an Enhanced Sensitivity to a PCNA-Derived Cell Permeable Peptide in Neuroblastoma Cells. *EBioMedicine* **2**, 1923–1931.
 31. Smith, S.J., Gu, L., Phipps, E.A., Dobroletcki, L.E., Mabrey, K.S., Gulley, P., Dillehay, K.L., Dong, Z., Fields, G.B., Chen, Y.R., et al. (2015). A Peptide mimicking a region in proliferating cell nuclear antigen specific to key protein interactions is cytotoxic to breast cancer. *Mol. Pharmacol.* **87**, 263–276.
 32. Angelis, K.J., Dusinská, M., and Collins, A.R. (1999). Single cell gel electrophoresis: detection of DNA damage at different levels of sensitivity. *Electrophoresis* **20**, 2133–2138.
 33. Maron, D.M., and Ames, B.N. (1983). Revised methods for the Salmonella mutagenicity test. *Mutat. Res.* **113**, 173–215.
 34. Dijt, F.J., Fichtinger-Schepman, A.M., Berends, F., and Reedijk, J. (1988). Formation and repair of cisplatin-induced adducts to DNA in cultured normal and repair-deficient human fibroblasts. *Cancer Res.* **48**, 6058–6062.
 35. Han, C., Srivastava, A.K., Cui, T., Wang, Q.E., and Wani, A.A. (2016). Differential DNA lesion formation and repair in heterochromatin and euchromatin. *Carcinogenesis* **37**, 129–138.
 36. Pommier, Y. (2006). Topoisomerase I inhibitors: camptothecins and beyond. *Nat. Rev. Cancer* **6**, 789–802.
 37. Oláh, J., Mulholland, A.J., and Harvey, J.N. (2011). Understanding the determinants of selectivity in drug metabolism through modeling of dextromethorphan oxidation by cytochrome P450. *Proc. Natl. Acad. Sci. USA* **108**, 6050–6055.
 38. Nair, A.B., and Jacob, S. (2016). A simple practice guide for dose conversion between animals and human. *J. Basic Clin. Pharm.* **7**, 27–31.
 39. Ma, M.K., Zamboni, W.C., Radomski, K.M., Furman, W.L., Santana, V.M., Houghton, P.J., Hanna, S.K., Smith, A.K., and Stewart, C.F. (2000). Pharmacokinetics of irinotecan and its metabolites SN-38 and APC in children with recurrent solid tumors after protracted low-dose irinotecan. *Clin. Cancer Res.* **6**, 813–819.
 40. Caudron-Herger, M., Müller-Ott, K., Mallm, J.P., Marth, C., Schmidt, U., Fejes-Tóth, K., and Rippe, K. (2011). Coding RNAs with a non-coding function: maintenance of open chromatin structure. *Nucleus* **2**, 410–424.
 41. Li, M., Xu, X., and Liu, Y. (2011). The SET2-RPB1 interaction domain of human RECQ5 is important for transcription-associated genome stability. *Mol. Cell Biol.* **31**, 2090–2099.
 42. Li, M., Pokharel, S., Wang, J.T., Xu, X., and Liu, Y. (2015). RECQ5-dependent SUMOylation of DNA topoisomerase I prevents transcription-associated genome instability. *Nat. Commun.* **6**, 6720.
 43. Luo, J., Solimini, N.L., and Elledge, S.J. (2009). Principles of cancer therapy: oncogene and non-oncogene addiction. *Cell* **136**, 823–837.
 44. Chang, H.R., Jung, E., Cho, S., Jeon, Y.J., and Kim, Y. (2021). Targeting Non-Oncogene Addiction for Cancer Therapy. *Biomolecules* **11**, 129.
 45. Jones, R.M., Mortusewicz, O., Afzal, I., Lavellec, M., García, P., Helleday, T., and Petermann, E. (2013). Increased replication initiation and conflicts with transcription underlie Cyclin E-induced replication stress. *Oncogene* **32**, 3744–3753.
 46. Li, H., Sandhu, M., Malkas, L.H., Hickey, R.J., and Vaidehi, N. (2017). How Does the Proliferating Cell Nuclear Antigen Modulate Binding Specificity to Multiple Partner Proteins? *J. Chem. Inf. Model.* **57**, 3011–3021.
 47. El Hage, A., French, S.L., Beyer, A.L., and Tollervey, D. (2010). Loss of Topoisomerase I leads to R-loop-mediated transcriptional blocks during ribosomal RNA synthesis. *Genes Dev.* **24**, 1546–1558.
 48. Guo, X., Chen, Z., Xia, Y., Lin, W., and Li, H. (2020). Investigation of the genetic variation in ACE2 on the structural recognition by the novel coronavirus (SARS-CoV-2). *J. Transl. Med.* **18**, 321.
 49. Morton, C.L., Wierdl, M., Oliver, L., Ma, M.K., Danks, M.K., Stewart, C.F., Eiseman, J.L., and Potter, P.M. (2000). Activation of CPT-11 in mice: identification and analysis of a highly effective plasma esterase. *Cancer Res.* **60**, 4206–4210.
 50. Sherman, W., Day, T., Jacobson, M.P., Friesner, R.A., and Farid, R. (2006). Novel procedure for modeling ligand/receptor induced fit effects. *J. Med. Chem.* **49**, 534–553.
 51. Capdeville, R., Buchdunger, E., Zimmermann, J., and Matter, A. (2002). Glivec (STI571, imatinib), a rationally developed, targeted anticancer drug. *Nat. Rev. Drug Discov.* **1**, 493–502.
 52. Emsley, P., Lohkamp, B., Scott, W.G., and Cowtan, K. (2010). Features and development of Coot. *Acta Crystallographica. Acta Crystallogr. D Biol. Crystallogr.* **66**, 486–501.
 53. Torices, R., and Munoz-Pajares, A.J. (2015). Phenix: An R Package to Estimate a Size-Controlled Phenotypic Integration Index. *Appl Plant Sci* **3**, apps1400104.
 54. Kabsch, W. Xds. (2010). *Acta Crystallographica Section D-Biological Crystallography* **66**, 125–132.
 55. McCoy, A.J., Grosse-Kunstleve, R.W., Adams, P.D., Winn, M.D., Storoni, L.C., and Read, R.J. (2007). Phaser crystallographic software. *J. Appl. Crystallogr.* **40**, 658–674.
 56. Yu, D.D., Andrali, S.S., Li, H., Lin, M., Huang, W., and Forman, B.M. (2016). Novel FXR (farnesoid X receptor) modulators: Potential therapies for cholesterol gallstone disease. *Bioorg. Med. Chem.* **24**, 3986–3993.
 57. Suzuki, Y., Holmes, J.B., Cerritelli, S.M., Sakhuja, K., Minczuk, M., Holt, I.J., and Crouch, R.J. (2010). An upstream open reading frame and the context of the two AUG codons affect the abundance of mitochondrial and nuclear RNase H1. *Mol. Cell Biol.* **30**, 5123–5134.
 58. Kabsch, W. (2010). Integration, scaling, space-group assignment and post-refinement. *Acta Crystallogr. D Biol. Crystallogr.* **66**, 133–144.
 59. Adams, P.D., Afonine, P.V., Bunkóczi, G., Chen, V.B., Davis, I.W., Echols, N., Headd, J.J., Hung, L.W., Kapral, G.J., Grosse-Kunstleve, R.W., et al. (2010). PHENIX: a comprehensive Python-based system for macromolecular structure solution. *Acta Crystallogr. D Biol. Crystallogr.* **66**, 213–221.
 60. Frum, R.A., Deb, S., and Deb, S.P. (2013). Use of the DNA fiber spreading technique to detect the effects of mutant p53 on DNA replication. *Methods Mol. Biol.* **962**, 147–155.
 61. Fouquier, J., and Guedj, M. (2015). Analysis of drug combinations: current methodological landscape. *Pharmacol. Res. Perspect.* **3**, e00149.
 62. Ramirez, P., Crouch, R.J., Cheung, V.G., and Grunseich, C. (2021). R-Loop Analysis by Dot-Blot. *J. Vis. Exp.*
 63. Sanz, L.A., and Chédin, F. (2019). High-resolution, strand-specific R-loop mapping via S9.6-based DNA-RNA immunoprecipitation and high-throughput sequencing. *Nat. Protoc.* **14**, 1734–1755.

STAR★METHODS

KEY RESOURCES TABLE

| REAGENT or RESOURCE | SOURCE | IDENTIFIER |
|---|------------------------------|---|
| Antibodies | | |
| Anti-H2A.X | Cell Signaling Tech. | Cat# 7631; RRID: AB_10860771 |
| Anti- γ H2A.X | Millipore | Cat# 05-636; RRID: AB_2755003 |
| Anti-phosphor-Chk1 | LifeSpan BioSciences | Cat# LS-C177888 |
| Anti-CAF-1 | Novus Biologicals | Cat# NB100-74608; RRID: AB_1048403 |
| Anti-MCM7 | Abcam | Cat# ab52489; RRID: AB_881187 |
| Anti-RNA/DNA hybrid (S9.6) | Millipore Sigma | Cat# MABE1095; RRID: AB_2861387 |
| Anti-dsDNA | Abcam | Cat# ab27156; RRID: AB_470907 |
| Anti-FLAG M2 affinity gel | Sigma | Cat# A2220; RRID: AB_10063035 |
| Anti-PCNA | Santa Cruz Biotechnology | Cat# SC-56; RRID: AB_628110 |
| Bacterial and virus strains | | |
| <i>E. coli</i> Rosetta 2 (DE3) | Sigma | Cat# 71397-3 |
| Biological samples | | |
| Mouse tumor tissues | This paper | N/A |
| Mouse plasma | This Paper | N/A |
| Chemicals, peptides, and recombinant proteins | | |
| ECL kit (West Pico PLUS Chemiluminescent Substrate) | ThermoFisher Scientific | Cat# 34080 |
| Lipofectamine 2000 | ThermoFisher Scientific | Cat# 11668027 |
| DMEM media | Corning | Cat# 10-013-CV |
| Fetal Bovine Serum | Neuromics | Cat# FBS002-HI |
| Penicillin/streptomycin (x100) | Corning | Cat# 30-002-CL |
| SYPRO orange dye | Sigma | Cat# S5692 |
| hEPM-1 Media Kit | Millipore | Cat# SCM201 |
| Sulforhodamine B | Sigma | Cat# 230162 |
| Benzonase | | |
| Small molecule compounds: AOH1996, AOH1996-1LE, and AOH1160-1LE | This paper | N/A |
| CellTiter-Glo assay | Promega | Cat# G7572 |
| Kolliphor EL | Sigma | Cat# C5135 |
| Poloxamer P124 | Spectrum Chemical Mfg. Corp. | Cat# P1168 |
| Crystal Violet | Sigma | Cat# C0775 |
| CPT-11 | Pfizer | Irinotecan hydrochloride |
| R9-caPep | Gu et al. ⁹ | N/A |
| Matrigel | BD Biosciences | Cat# 354248 |
| Critical commercial assays | | |
| <i>In Situ</i> Cell Death Detection | Roche-applied Science | Cat# 12156792910 |
| NCI-60 cell panel screen | National Cancer Institute | https://ntp.cancer.gov/discovery_development/nci-60/ |
| BCA protein assay kit | ThermoFisher Scientific | Cat# PI23227 |
| QuickChangell Site Directed Mutagenesis kit | Agilent | Cat# 200523 |
| Deposited data | | |
| Co-crystal structure of caPCNA bound to AOH1160 derivative | PDB | 7N92 |
| Experimental models: Cell lines | | |
| SK-N-DZ | ATCC | Cat# CRL-2149 |

(Continued on next page)

Continued

| REAGENT or RESOURCE | SOURCE | IDENTIFIER |
|---------------------|------------|---------------|
| SK-N-BE(2)c | ATCC | Cat# CRL-2271 |
| SK-N-AS | ATCC | Cat# CRL-2137 |
| MDA-MB-468 | ATCC | Cat# HTB-132 |
| SH-SY5Y | ATCC | Cat# CRL-2266 |
| 7SM0032 | Millipore | Cat# SCR223 |
| HEK293-FLAG-PCNA | This paper | N/A |

Experimental models: Organisms/strains

| | | |
|------------------------|-----------------------------------|-----|
| ES1 ⁹ /SCID | Morton, C.L. et al. ⁴⁷ | N/A |
|------------------------|-----------------------------------|-----|

Oligonucleotides

| | | |
|---|------------|-----|
| PCNA-CR1: GGACTCGTCCCACGTCTCTT | This paper | N/A |
| PCNA-CR4: CTTTGGTGCAGCTCACCCCTG | This paper | N/A |
| PCNA-SvF: CGGCATTAAACGGTTGCAGG | This paper | N/A |
| PCNA-SvR: CGTGGCAGGCCAATGAGAAG | This paper | N/A |
| PCNA-FA-FP: ACGAGGCCTGCTGGGATATT | This paper | N/A |
| PCNA-FA-FP: TGAGGGCTAGGCTCGAAAGC | This paper | N/A |
| RPB1-CR1: ATTGTCTCGGATGATGTACT | This paper | N/A |
| RPB1-APIM: CCAGTACCCAGGCGC CAAGGCCATCATCCGAGACAATGGT | This paper | N/A |

Recombinant DNA

| | | |
|--|---------------------------------|---------------|
| pET22b-hPCNA | This paper | N/A |
| FLAG-PCNA expression plasmid (NM_002592) | Origene | Cat# RC201741 |
| hRNASEH1-M27-GFP | Suzuki, Y. et al. ⁴⁸ | N/A |
| p3XFLAG-RPB1 | This paper | N/A |
| p3XFLAG-RPB1-Mut | This paper | N/A |
| pX458-PCNA-CR1/4 | This paper | N/A |

Software and algorithms

| | | |
|--|---|---|
| NAMD | Phillips et al. ⁴⁹ | N/A |
| MetaCore | Clarivate Analytics | https://clarivate.com |
| GraphPad Prism 8 | GraphPad Software | www.graphpad.com |
| PyMol (The PyMoL Molecular Graphics System, Version 2.0) | Schrödinger, LLC | https://www.schrodinger.com/products/pymol |
| LiAn (Legion Interfaces Analysis) program | Guo et al. ⁵⁰ | N/A |
| All-Around Docking | Yu et al. ⁵¹ | N/A |
| FlowJo | FlowJo, LLC | https://www.flowjo.com |
| Crystallographic Object-Oriented Toolkit (Coot) | Emsley et al. ⁵² | N/A |
| Phenix | Torices et al. ⁵³ | N/A |
| XDS | Kabsch W. ⁵⁴ | N/A |
| Phaser | McCoy, et al. ⁵⁵ | N/A |
| Molecular Operating Environment (MOE) | Chemical Computing Group ULC, 1010 Sherbooke St. West, Suite #910, Montreal, QC, Canada, H3A 2R7, 2023. | https://www.chemcomp.com/index.htm |

Deposited data

| | | |
|--|------------|-------------|
| Co-crystal structure of PCNA:AOH1160-1LE | This paper | PDBID: 8GL9 |
| Co-crystal structure of PCNA:AOH1996-1LE | This paper | PDBID: 8GLA |

RESOURCE AVAILABILITY

Lead contact

Further information and requests for resources and reagents generated in this study should be directed to the Lead Contact, Dr. Linda H. Malkas (Lmalkas@coh.org).

Materials availability

All cell lines and unique reagents generated in this study are available from the [lead contact](#) with a completed Materials Transfer Agreement.

Data and code availability

- Protein-ligand crystallization data have been deposited at Protein Data Bank archive and are publicly available as of the date of publication. Accession numbers are listed in the [key resources table](#).
- This paper does not report any original code.
- Any additional information required to reanalyze the data reported in this paper is available from the [lead contact](#) upon request.

EXPERIMENTAL MODEL AND STUDY PARTICIPANT DETAILS

Plasmids and cell lines

RPB1 cDNA from pBs-RPB1A-GFP-RPB1 (a kind gift from Dr. Marteiijn; PMID: 29632207) was cloned into p3XFLAG-CMV-7.1 (Sigma Aldrich, #E7533) to create the p3XFLAG-RPB1 plasmid, which expresses FLAG-tagged RPB1. p3XFLAG-RPB1-Mut expressing APIM-mutated RPB1 was generated by mutagenesis using QuickChange Site Directed Mutagenesis kit purchased from Agilent (Santa Clara, CA) and RPB1-APIM oligo as the mutagenesis primer.

Human neuroblastoma cell lines (SK-N-DZ, SK-N-BE(2)c, SK-N-AS, and SH-SY5Y) and breast cancer cell line (MDA-MB-468) were obtained from American Type Culture Collection (ATCC) and cultured in DMEM with 10% fetal bovine serum (FBS), 100 units/ml penicillin, and 100 μ g/ml streptomycin. The HEK293T cells were cultured in DMEM with 10% fetal bovine serum (FBS), 100 units/ml penicillin, and 100 μ g/ml streptomycin. The Human embryonic progenitor cell line 7SM0032 was acquired from Millipore and cultured in the hEPM-1 Media Kit purchased from the same company. The HEK293 cell line stably expressing the FLAG-tagged human PCNA (HEK293-FLAG-PCNA) was created by single colony selection and screening after transfecting HEK293 cells with a plasmid (NM_002592) purchased from Origene (Rockville, MD). All cells were grown at 37°C in the presence of 5% CO₂.

Animals

A breeding colony of ES1^e/SCID mice, originally provided by Dr. Philip M. Potter of the St. Jude Children's Research Hospital,⁴⁹ was maintained at City of Hope. All experiments involving live animals were carried out in strict accordance with the recommendations stated in "the Guide for the Care and Use of Laboratory Animals", as adopted and promulgated by the National Institutes of Health. The protocol (#11034) was reviewed and approved by the City of Hope Institutional Animal Care and Use Committee. Studies were performed in mice of both sexes between 5 and 10 weeks old, except for studies of breast cancers, which involved only female mice.

METHODS DETAILS

Computer modeling

The computer modeling of AOH1996 binding to PCNA was based on the All-Around-Docking methodology and refined by 50ns meta-dynamic simulation using NAMD software.⁵¹ The Gibbs free energy (ΔG) determined by the docking study was related to the compound's K_i which was determined using the Nernst equation at system equilibrium: $\Delta G = -RT \ln(K_i)$, in which $R = 0.001987$ kcal/K/mol. To model AOH1996 interaction with PCNA in complex with RPB1, we downloaded the protein structures: PDB 5iyd for the RPB1 APIM motif peptide and 5mlw for PCNA in complex with ZRANB3 APIM motif peptide, from the RCSB Protein Data Bank. The peptide structural alignment of RPB1 and ZRANB3 APIM motif peptides is carried out using PyMol (The PyMOL Molecular Graphics System, Version 2.0 Schrödinger, LLC). The best binding pocket of AOH1996 to the PCNA/RPB1 complex is predicted by using our in-house developed All-Around Docking method,⁵⁶ which automatically docks the ligand all-around the protein surface to search for the best sites by Glide²⁵ and Induced Fitting docking⁵⁰ methods. The 2-dimensional interaction diagram is drawn by Schrödinger Maestro software. The 3-dimensional interaction plot is generated by our in-house developed LiAn (Legion Interfaces Analysis) program,⁴⁸ which calculates and displays protein-ligand or protein-protein interactions (such as hydrogen bond, salt-bridge, water-bridge, π -interactions, hydrophobic interactions, halogen bond, etc.) for single protein structure or massive structures from molecular dynamic simulations.

Transfection

The plasmids expressing a FLAG-tagged PCNA (NM_002592), FLAG-tagged RPB1 (p3XFLAG-RPB1), FLAG-tagged RPB1 with mutated APIM domain (p3XFLAG-RPB1-Mut), or the human RNase H1 gene⁵⁷ were transfected by Lipofectamine 2000 (ThermoFisher Scientific).

Purification and crystallization of PCNA

Human PCNA in a pET22b-hPCNA vector was transformed into *E. coli* Rosetta 2 (DE3) cells. PCNA expression was induced by 0.4 mM IPTG, OD₆₀₀=0.6, and cells were grown for 5 hrs at 37°C. Cells were harvested by centrifugation for 30 min at 5,000 x g, and the pellet was resuspended in lysis buffer containing 25 mM Tris-HCl pH 8.5, 50 mM NaCl, 1 mM β -mercaptoethanol, 1 mM

PMSF and 10% glycerol. Cells were sonicated, and soluble hPCNA in the cell supernatant was purified using a HiTrap Q FF column (GE Healthcare) in lysis buffer containing a 0.05 - 1.0 M NaCl gradient, followed by anion exchange chromatography using ENrichQ (BioRad) using lysis buffer over a 0.15-1.0 M NaCl gradient. Pooled PCNA fractions were loaded onto a HiLoad 26/60 Superdex 200 gel filtration column (GE Healthcare), suspended in 10 mM HEPES pH 7.4, 100 mM NaCl and 1 mM β -mercaptoethanol. Purified hPCNA protein was incubated overnight with the AOH1160-1LE compound at 9 mg/mL PCNA (313 μ M), 4 mM AOH1160-1LE, in 9 mM HEPES pH 7.4, 90 mM NaCl, and 10% DMSO.

Thermal denaturation assay for PCNA-AOH1996 interaction

The assay was performed using a BioRad CFX Connect Real-Time PCR Detection System. Protein (PCNA), inhibitors (AOH1996 and AOH1160-1LE), and 200x SYPRO orange dye (Sigma) were diluted into phosphate buffered saline (PBS). The final concentration of recombinant PCNA was 9 μ M, and the final compound concentrations were at 0, 10, or 30 μ M. Sample plates were heated from 25°C to 95°C with heating increments of 0.5 °C/min. Fluorescence intensity was measured within the excitation/emission ranges 470-505/540-700 nm.

Crystallization and X-ray data analysis

Co-crystals were grown by vapor diffusion, with a reservoir solution of 100 mM sodium cacodylate pH 6.5, 200 mM NaCl and 2.0 M ammonium sulfate. Crystals after two weeks growth at 293°K were crushed using the Seed Bead Kit (Hampton Research) and a 10⁻⁵ seed dilution in a 1:1 ratio with pre-incubated PCNA:AOH1160-1LE or PCNA:AOH1996-1LE was setup in hanging drop vapor diffusion, using the same reservoir solution. Seeded crystals grown at 293°K were collected and flash frozen in liquid N₂. X-ray data was collected at beamline 9-2 SSRL, Stanford, CA at 100°K. Images were collected at 0.2 sec, 0.15 deg per image, over 270 deg of data. Data was processed using XDS⁵⁸ to 2.81 Å in the H3 space group, with unit cell dimensions of a=b=197.14 Å, c=126.98 Å, a=b= 90° and c=120° for PCNA:AOH1160-1LE. Data for PCNA:AOH1996-1LE was processed to 3.77 Å, with an H3 space group with unit cell dimensions of a=b=199.49 Å, c=129.41 Å, a=b= 90° and c=120°. Phasing was obtained using Phaser-MR⁵⁵ with 3VKX.pdb as the search model. Model building and refinement was completed using Phenix⁵⁹ and Coot.⁵² Images of molecular interactions were prepared utilizing the MOE (Molecular Operating Environment, version 2020.0101, Chemical Computing Group, Ontario, Canada). The PCNA:AOH1160-1LE and the PCNA:AOH1996-1LE co-crystal structures have been deposited in the PDB, with PDB codes XYZ and XYZ, respectively.

Establishment of mutant cell lines by CRISPR

To introduce establish SK-N-AS cells heterozygous or homozygous of the mutant PCNA allele (L47V), specific guide RNAs (sgRNAs) were designed using the online tool CHOPCHOP (<http://chopchop.cbu.uib.no>). sgRNA sequences were selected close to the target sequence and with minimal identical genomic matches or near-matches to reduce risk of off-target effects. After confirming CRISPR editing efficiency, two sgRNAs were synthesized (**PCNA-CR1**: GGACTCGTCCCACGTCTCTT and **PCNA-CR4**: CTTTGGTG CAGCTCACCTG). According to the sgRNA cutting sites, two mutations were made in the protospacer adjacent motif (PAM) sequence of the homology-directed repair (HDR) donor template to prevent re-cutting by CRISPR. The primer set (**PCNA-SvF**: CGGCATTAAACGGTTGCAGG and **PCNA-SvR**: CGTGGCAGGCCAATGAGAAG) was used to perform the surveyor assay and DNA amplification. The primer set (**PCNA-FA-FP**: ACGAGGCTGCTGGGATATT and **PCNA-FA-RP**: TGAGGGCTAGGCTCG AAAGC) was used for DNA sequencing. The SK-N-AS neuroblastoma cells were seeded at a density of 5x10⁵/well in a 6-well plate and were co-transfected with: 1) pX458-PCNA-CR1/4 plasmid encoding CRISPR Sp-CAS9, a GFP selection marker, and the PCNA-CR1 and PCNA-CR4 sgRNAs, and 2) a plasmid containing the mCherry selection marker and the donor template. 48 h later, transfected cells were sorted for GFP and mCherry expression and enriched cells were seeded into 96-well plates by single cell limiting dilution. Single-cell clones were screened by DNA sequencing of the target site to identify cells homozygous (**PCNA^{L47V/L47V}**) or heterozygous (**PCNA^{+/L47V}**) for the mutant allele. The RPB1 mutant cell lines were established by the same method using **RPB1-CR1**: ATGTCTCGGATGATGTACT as sgRNA.

Cell cycle analysis

Cells were seeded in a 6-well plate at 1x10⁵/ml. After treatment with the compound, cells were fixed in 60% ethanol and stained with propidium iodide (PI). PI fluorescence intensity within the cells was measured by flow cytometry, and the data was analyzed using the FlowJo program.

Cell growth and apoptosis assays

Cells were seeded at 5 x 10³/ml or 3 x 10⁴/ml into a 96-well plate, depending on the cell lines, and were treated with various concentrations of AOH1996 for 72 h after being allowed to attach overnight. Cell growth was measured by the CellTiter-Glo assay (Promega) according to the manufacturer's instruction. Alternatively, cell growth was analyzed by the IncuCyte® S3 Live-cell Analysis Systems (Sartorius), which measures cell confluence by periodic imaging. The National Cancer Institute (NCI) examined the effect of AOH1996 on the NCI60 panel of cell lines using the standard 5-dose assay containing sulforhodamine B (SRB). The assay is described in more details at (https://dtp.cancer.gov/discovery_development/nci-60/methodology.htm). The 50% growth inhibition concentration (GI₅₀) was calculated by the NCI.

Cell apoptosis was measured on a chamber slide at a seeding density of 1×10^5 /ml. After treatment with 500 nM AOH1996 for 24 h, cells were fixed and analyzed using the terminal deoxynucleotidyl transferase-mediated dUTP nick end labeling (TUNEL) assay containing TMR red *in situ* cell death detection kit (Roche Diagnostics).

DNA combing analysis

A DNA combing assay was performed as described.⁶⁰ Briefly, synchronized neuroblastoma (SK-N-BE(2)-C) or breast cancer (MDA-MB-231) cells were incubated first with 5-Chloro-2'-deoxyuridine (CldU) for 10 minutes. After washing away the unincorporated CldU, cells were incubated with 5-Iodo-2'-deoxyuridine (IdU), in the absence or presence of AOH1996 at the indicated concentrations for 20 minutes. The cells were spotted and lysed on microscope slides. The DNA fibers spread across the slides were immunologically stained with fluorophore-conjugated antibodies specific for CldU and IdU, and were visualized under a fluorescent microscope. The length of CldU and IdU incorporated DNA fibers was measured using ImageJ software (National Institute of Health).

Clonogenic assay

SK-N-DZ neuroblastoma cells were seeded and allowed to attach onto 60-mm plates (300 per plate). Cells were treated with cisplatin alone or with cisplatin and AOH1996 for 18 h. Cells were then cultured in fresh medium without cisplatin or AOH1996 for 18 d to allow the surviving cells to form colonies. The colonies were stained with 0.5% crystal violet and counted. Synergy between AOH1996 and cisplatin was evaluated using combination indices (CI) based on the Bliss independence model $[CI = (E_A + E_B - E_A * E_B) / E_{AB}]$.⁶¹

Western and dot blot

Cells were dissolved into Laemmli sample buffer on the plate. Whole cell extracts were sonicated, resolved on a 4–12% Bis-Tris protein gel, and blotted onto a nitrocellulose membrane. The membrane was blocked with 5% nonfat dry milk and incubated individually with antibodies for H2A.X (Cell Signaling Technology, Danvers, MA), γ H2A.X (Millipore), CAF-1 (Novus Biologicals), PCNA (Santa Cruz Biotechnology), and MCM7 (Abcam) diluted in blocking buffer. After incubation with peroxidase-conjugated secondary antibodies, the protein of interest was detected using an ECL kit purchased from ThermoFisher Scientific.

For dot blot detection of R-loop, cells were treated with various concentrations of AOH1996 for 24 hours. Genomic DNAs were purified as described.⁶² Genomic DNAs were applied onto a nitrocellulose membrane and R-loop levels were analyzed by S9.6 antibody.^{63,47} Total genomic DNA were measured by a double stranded DNA specific antibody purchased from Abcam (Cambridge, United Kingdom).

All semi-quantitative blotting studies, including dot blotting, western blotting, and IP-western blotting were performed at least twice to ensure reproducibility.

Cell fractionation and immunoprecipitation

Cells were fractionated as previously described.²⁴ Briefly, intact nuclei isolated following osmotic lysis were homogenized using a 21G needle. Chromatin was pelleted by centrifugation and incubated overnight at 4°C with benzonase in two volumes of nuclease buffer (20 mM HEPES pH 7.5, 1.5 mM MgCl₂, 1 mM EDTA, 150 mM KCl, 10% glycerol, 0.5 U μ l⁻¹ benzonase). The resulting supernatant was collected as the chromatin bound (CB) fraction. Alternatively, we sequentially incubated the chromatin pellet with RNase A and benzonase and collected the supernatants after each digestion as the CB:RNA+ and CB:RNA- fractions, respectively.²⁴ The chromatin extracts (CB) were incubated overnight with Anti-FLAG M2 affinity gel (Sigma) at 4°C to pull down FLAG-tagged PCNA.

Compound metabolism in liver microsome

AOH1160 analogs were incubated at 37°C with human liver microsomes in the absence or presence of NADPH. An aliquot of the reaction mixture was then taken after various incubation times, and the Concentration of Compound determined by liquid chromatography–tandem mass spectrometry (LC-MS/MS) as previously described.¹⁷

Proteomic analysis using mass spectrometry

SK-N-AS cells homozygous for the wildtype or mutant RPB1 allele were treated with or without 0.5 μ M AOH1996 overnight. Cell pellets were dissolved in 100 μ L lysis buffer (0.5 M triethylammonium bicarbonate, 0.05% sodium dodecyl sulfate) and subjected to tip sonication. Protein lysates were quantified for protein content using the BCA protein assay kit (Thermo Fisher Scientific, Waltham, MA, USA) and equal amounts of protein were used per condition, adjusted to the highest volume with lysis buffer. Proteins were then reduced [4 μ L of 100mM methyl methanethiosulfonate (MMTS), 60°C for 1 hour], alkylated [2 μ L of 100mM tris(2-carboxyethyl)phosphine (TCEP), room temperature for 10 min] and enzymatically digested overnight [1:25 trypsin/LysC, 37°C in dark]. Peptides were labelled using the 16-plex TMT reagents (TMT labels dissolved in 41 μ L anhydrous acetonitrile and transferred to each sample, at room temperature for 2 hr) (Thermo Fisher Scientific, Waltham, MA, USA). The labelling scheme was as follows: 126=untreated 1, 127N=treated 1, 127C=untreated 2, 128N=treated 2, 128C=untreated 3, 129N=treated 3, 129C=untreated 4, 130N=treated 4, 130C=26-0h-1, 131N=26-0h-2, 131C=26-24h-1, 132N=26-24h-2, 132C=31-0h-1, 133N=31-0h-2, 133C=31-24h-1, 134N=31-24h-2. The labelling reaction was stopped with the additions of 8 μ L of 5% hydroxylamine in each sample and incubating at room temperature for 10 min. Peptides from all samples were then mixed and phospho-enrichment was performed using the Sequential enrichment of metal oxide affinity chromatography (SMOAC) protocol (Thermo Fisher Scientific, Waltham, MA, USA). Normalization was performed on total peptide amount and scaling was performed on all averages. The scaled abundance data

was analyzed by the GO Process enrichment of MetaCore (Clarivate, Philadelphia, PA) with cutoff thresholds having a p-value (moderated t-test) less than 0.05 and a fold change (FC) greater than 2.

Pharmacokinetic (PK) study in animals

An oral dosing solution was prepared by dissolving AOH1996 (40 mg) in a mixture of Kolliphor EL (840 mg) and Poloxamer P124 (120 mg). For the mouse study, blood samples were collected from ES1^o/SCID mice (3 male and 3 female) per dosing group by cardiac puncture at 10, 20, and 30 min and 1, 2, 4, 6, and 24 h after dosing. For the dog study, blood samples were collected from 3 male beagle dogs per dosing group by venipuncture of peripheral veins at 5, 15, and 30 min and 1, 2, 4, 8, 12, and 24 h after dosing. Following removal of blood cells, plasma concentration of AOH1996 was determined by LC-MS/MS as described.¹⁷ Oral PK was determined using standard non-compartmental methods.

In vivo tumor model

Compounds were tested in the ES1^o/SCID mice, originally provided by Dr. Philip M. Potter of the St. Jude Children's Research Hospital.⁴⁹ SK-N-BE(2)c and SK-N-AS neuroblastoma cells were suspended in Matrigel (BD Biosciences) at 5×10^7 /ml and 4×10^7 /ml, respectively, after being harvested and washed twice in PBS. The cell suspension (0.1 mL) was subcutaneously injected into the right flank of each ES1^o/SCID mouse. AOH1996 was dosed orally. CPT-11 was given by intraperitoneal injection. Tumor size and animal weight were measured weekly. At the end of the experiment, tumors were isolated from sacrificed mice and analyzed by immunohistochemistry staining with antibodies specific for phosphor-Chk1 and γ H2A.X.

QUANTIFICATION AND STATISTICAL ANALYSIS

The cell apoptosis data in Figure 3B, the cell growth inhibition data in Figures 3C and 3D, the tumor growth inhibition data in Figures 4C–4E, and the DNA combing assay data in Figure 7B were analyzed by the Student's *t*-test using the Microsoft Excel program. The animal survival data in Figure 4H was analyzed by the Log-rank (Mantel-Cox) test using the GraphPad Prism 8 program.

Cell Chemical Biology, Volume 30

Supplemental information

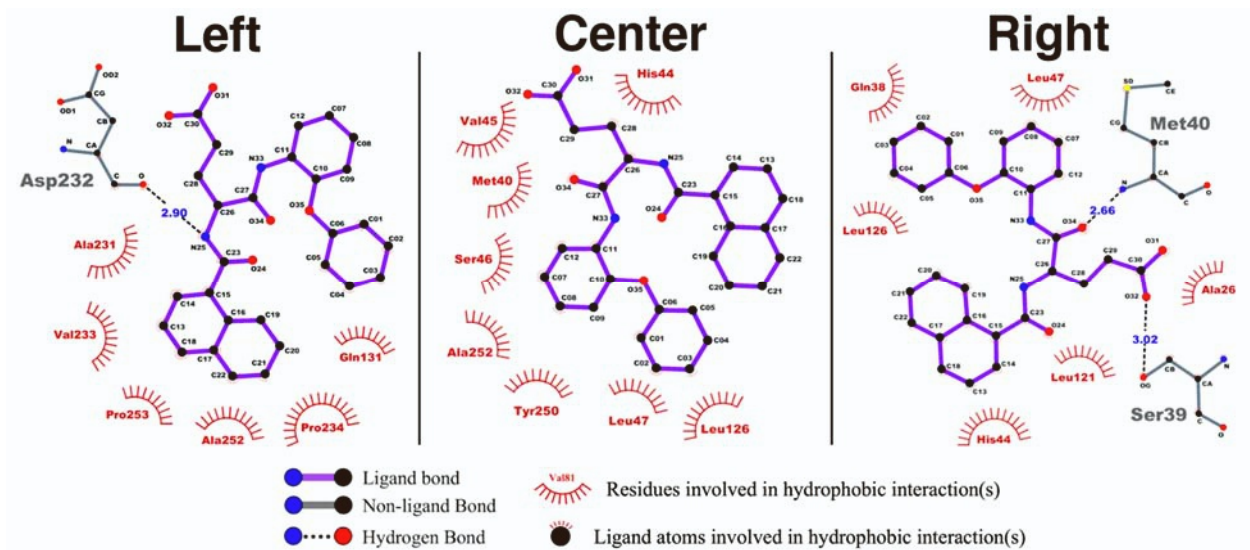
**Small molecule targeting
of transcription-replication conflict
for selective chemotherapy**

Long Gu, Min Li, Caroline M. Li, Pouya Haratipour, Robert Lingeman, Jennifer Jossart, Margarita Gutova, Linda Flores, Caitlyn Hyde, Nikola Kenjić, Haiqing Li, Vincent Chung, Hongzhi Li, Brett Lomenick, Daniel D. Von Hoff, Timothy W. Synold, Karen S. Aboody, Yilun Liu, David Horne, Robert J. Hickey, J. Jefferson P. Perry, and Linda H. Malkas

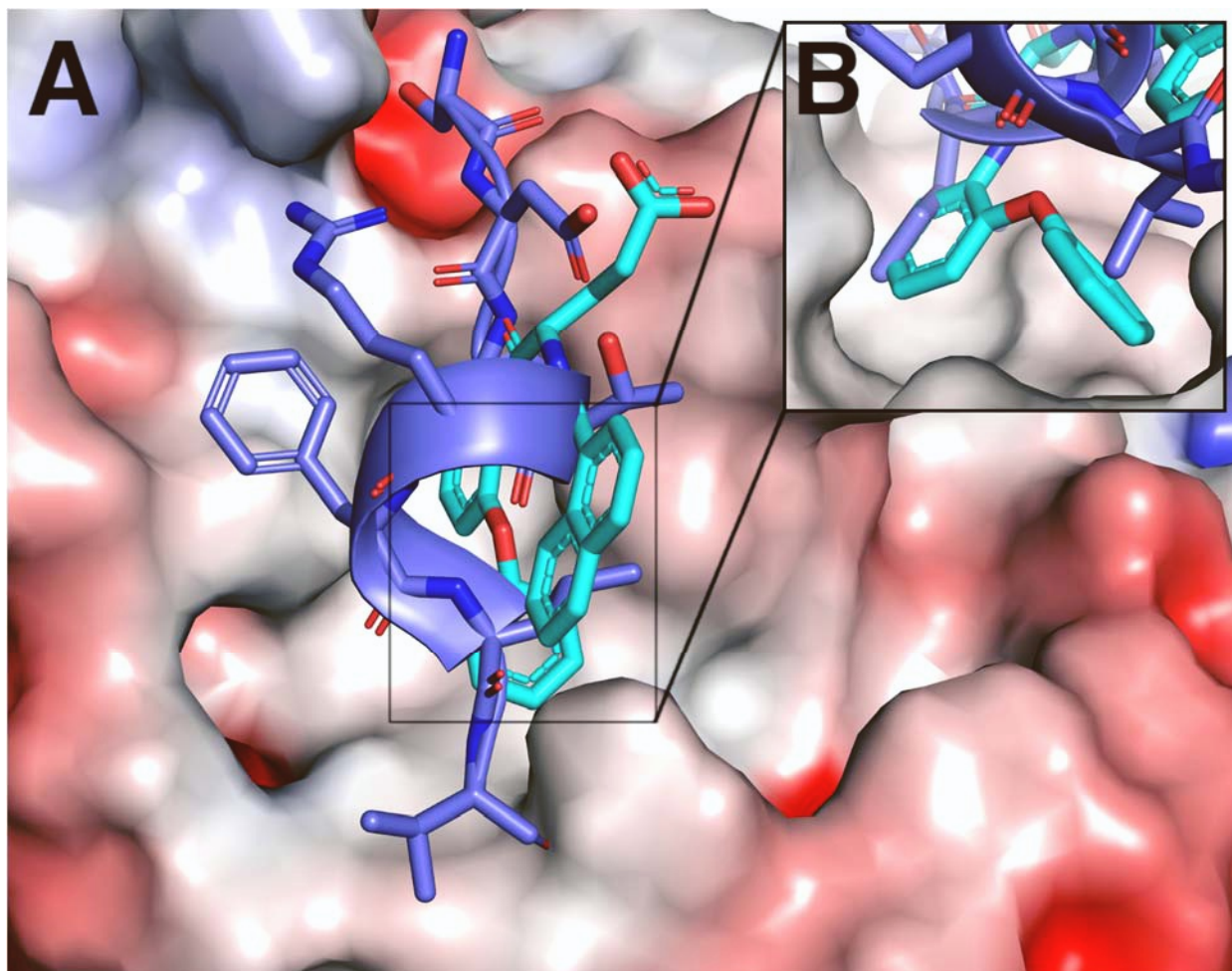
| | PCNA-AOH1160LE | PCNA-AOH1996LE |
|--|----------------------------|----------------------------|
| Data collection | | |
| Beamline | SSRL 9-2 | SSRL 9-2 |
| Wavelength (Å) | 0.98 | 0.98 |
| Space group | H3 | H3 |
| Cell dimensions; <i>a</i> , <i>b</i> , <i>c</i> (Å), (°) | 197.14, 197.14, 126.98 | 199.49, 199.49, 129.41 |
| Resolution (Å) | 37.96 - 2.81 (2.91 - 2.81) | 38.51 - 3.77 (3.91 - 3.77) |
| R_{merge}^a | 0.113 (0.954) | 0.1797 (0.9186) |
| Total reflections | 351626 (34837) | 114061 (27122) |
| Mean ($\langle I \rangle / \sigma(I)$) | 12.9 (2.0) | 8.72 (2.0) |
| CC _{1/2} | 0.994 (0.740) | 0.995 (0.678) |
| Completeness (%) | 99.71 (99.87) | 99.7 (99.7) |
| Redundancy | 7.8 (7.5) | 5.9 (5.8) |
| Refinement | | |
| Resolution (Å) | 37.96 - 2.81 (2.91 - 2.81) | 38.51 - 3.77 (3.91 - 3.77) |
| R_{work}^b | 0.1981 (0.3083) | 0.2051 (0.2787) |
| R_{free}^c | 0.2400 (0.3884) | 0.2590 (0.3527) |
| Unique reflections | 44702 (4439) | 19308 (1920) |
| No. of non-hydrogen atoms | 7639 | 7571 |
| Protein | 7414 | 7341 |
| Ligand | 218 | 230 |
| Solvent | 7 | 0 |
| RMS deviation bonds (Å) | 0.010 | 0.004 |
| RMS deviation angles (°) | 1.23 | 0.70 |
| Overall mean B-factor (Å ²) | 56.95 | 97.39 |
| Macromolecule | 57.06 | 97.45 |
| Ligand | 53.70 | 95.39 |
| Solvent | 43.28 | - |
| <u>Ramachandran plot analysis</u> ^e | | |
| Favored region | 95.88 | 93.52 |
| Allowed region | 3.80 | 5.93 |
| Outlier region ^d | 0.33 | 0.55 |
| Rotamer outlier | 2.38 | 0.24 |
| Clash score | 8.34 | 11.88 |

^a $R_{\text{merge}} = \sum_h |I_h - \langle I \rangle| / \sum_h I_h$, where I_h is the intensity of reflection h , and $\langle I \rangle$ is the mean intensity of all symmetry-related reflections ^b $R_{\text{work}} = \sum ||F_o| - |F_c|| / \sum |F_o|$, F_o and F_c are observed and calculated structure factor amplitudes. ^cFive percent of the reflections were reserved to create an R_{free} test set used during each subsequent round of refinement. ^dOutlier regions belongs to three residues that in the N-terminal of the protein in the crystal interface of two monomers. Data for the highest resolution shell is shown in brackets.

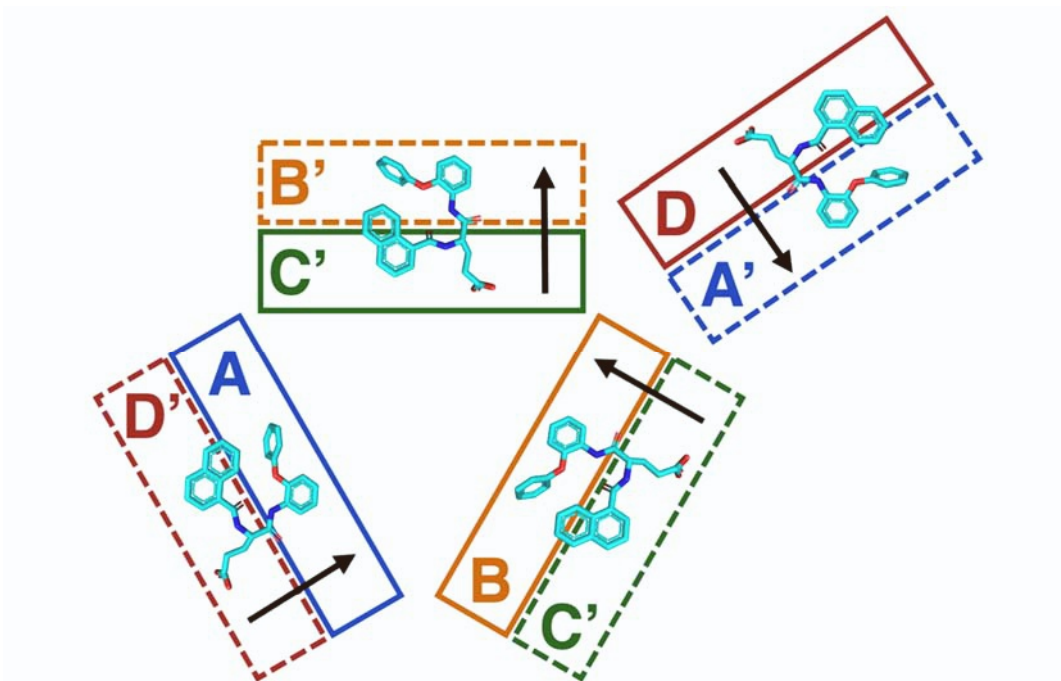
Supp. Table S1 (related to Figure 1): Crystallographic data and refinement statistics.



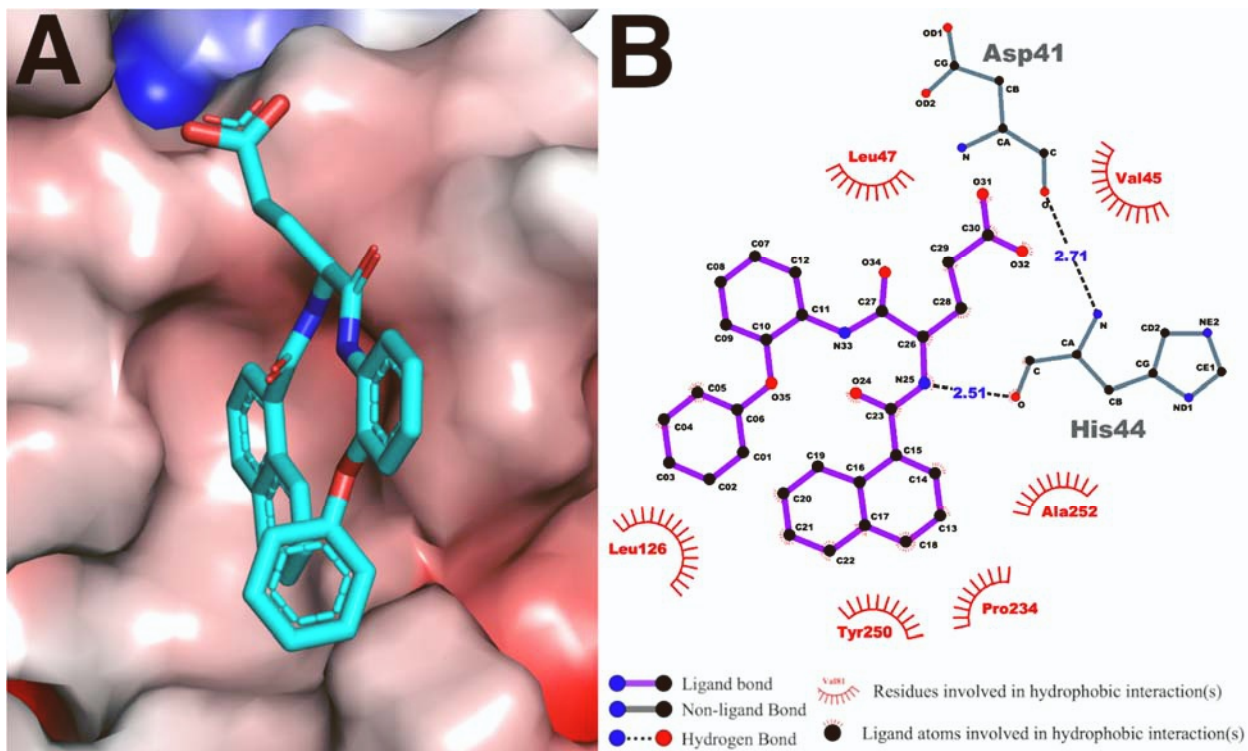
Supplementary Figure S1 (related to Figure 1): Schematic of AOH1160-1LE molecule interactions with PCNA. Individual AOH1160-1LE molecules are listed from left to right based on their positioning in the PIP box pocket as shown in Figure 1. Specific protein-ligand interactions are highlighted based on the provided legend.



Supplementary Figure S2 (related to Figure 1): Structural superimposition of PCNA:AOH1160-1LE and PCNA:APIM peptide complexes bound to PCNA. A.) The central AOH1160-1LE, cyan binds to the same hydrophobic pockets as the ZRANB3 APIM peptide (PDB code: 5YD8) colored in purple. B.) Close up view of the two hydrophobic binding regions of PCNA, with the diphenyl ether of central AOH1160-1LE positioned where Ile1072 and Val1077 of APIM peptide bind.

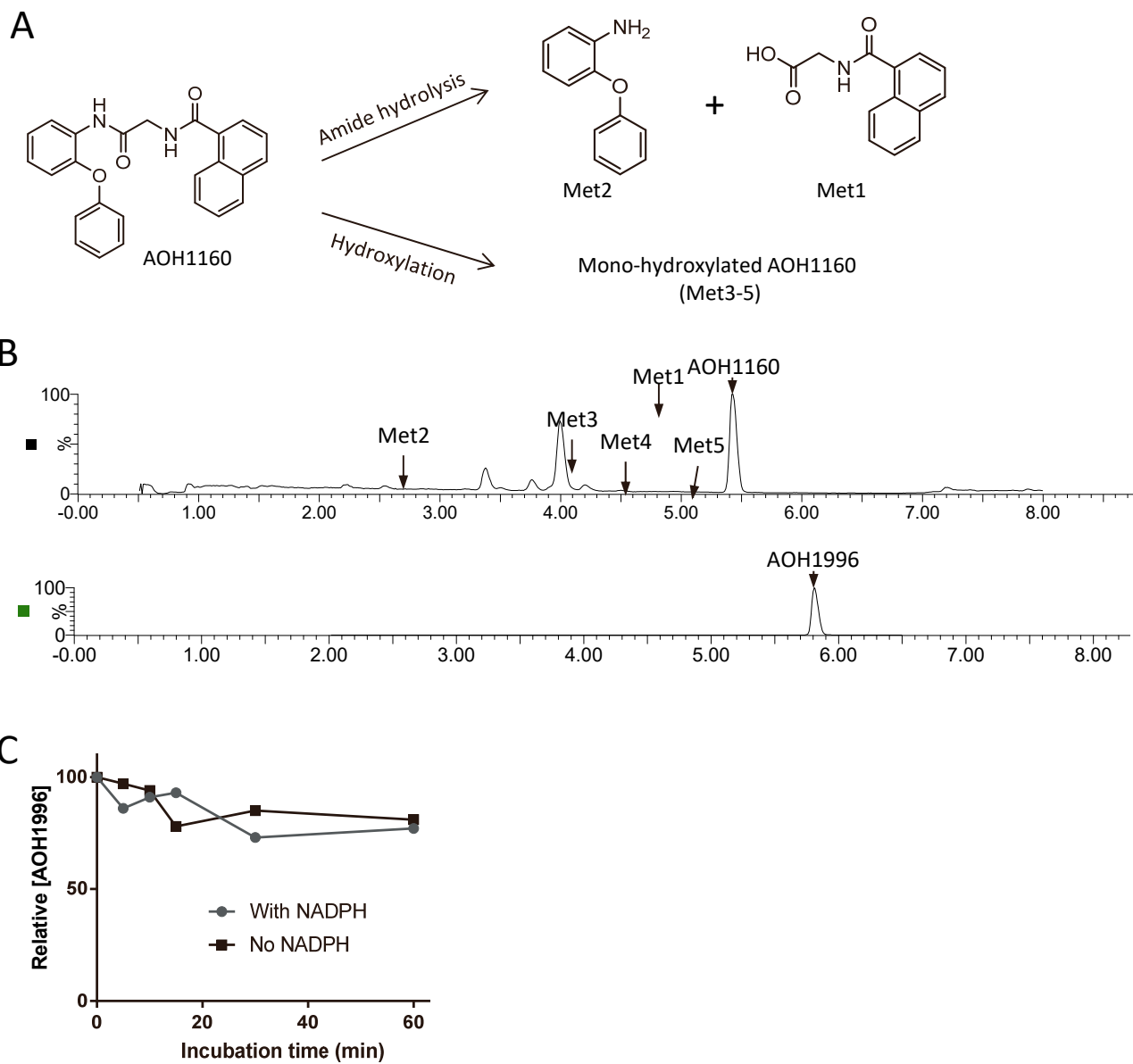


Supplementary Figure S3 (related Figure 1): Orientation of AOH1160-1LE bound into PIP box cavity of PCNA. Chains A-D are depicted by solid boxes, with corresponding symmetry mates in dashes, each labeled accordingly. The orientation of the central AOH1160-1LE diphenyl ether binding is depicted and further indicated by the direction of the black arrows.



Supplementary Figure S4 (related to Figure 1): Chain C central AOH1160-1LE molecule interactions with PCNA, via the naphthalene group. Specific protein-ligand interactions are highlighted based on the provided legend.

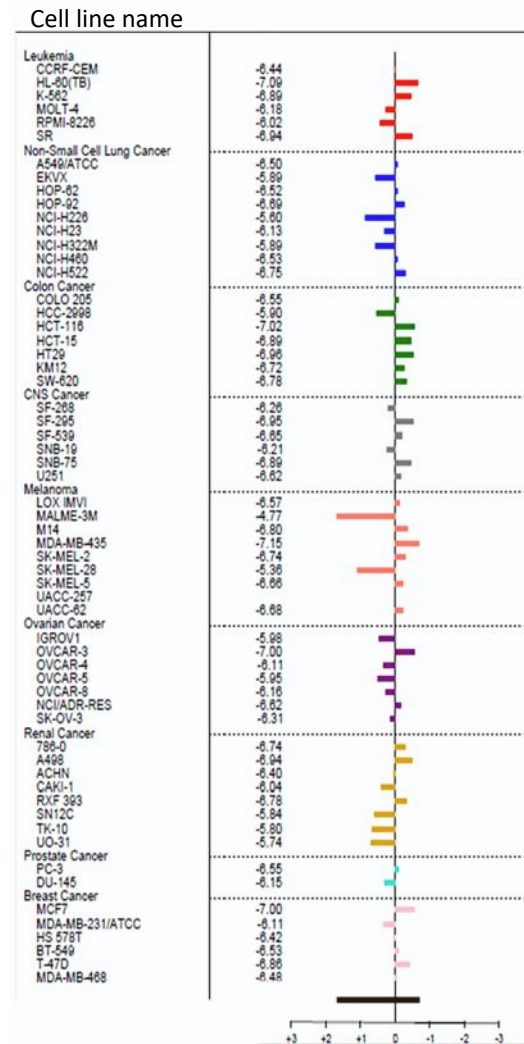
Supp Figure S5



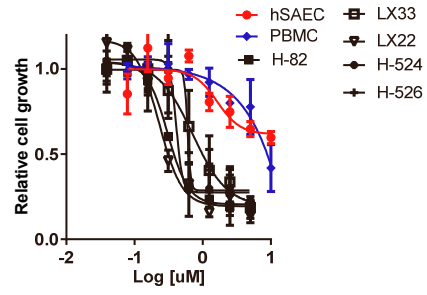
Supplemental Figure S5 (related to Figure 2 and Figure 4): AOH1996 metabolism and *in vivo* pharmacokinetics: A) Illustration of AOH1160 degradation by carboxyl esterase-mediated cleavage or by hydroxylation. **B)** Chromatogram of liver microsome reaction mixtures of AOH1160 and AOH1996. The metabolites shown in **(A)** are indicated above their corresponding peaks. **C)** An aliquot of the liver microsome reaction mixture of AOH1996 was taken after various incubation times in the presence or absence of NADPH as the energy source. AOH1996 concentrations, determined by LC/MS-MS, as a percentage of the input concentration were graphed.

Supp Figure S6

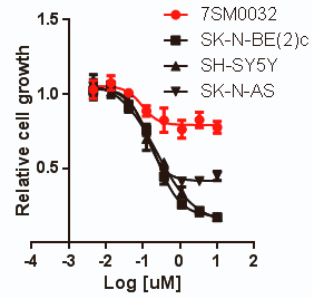
A



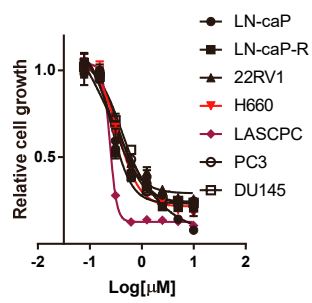
B



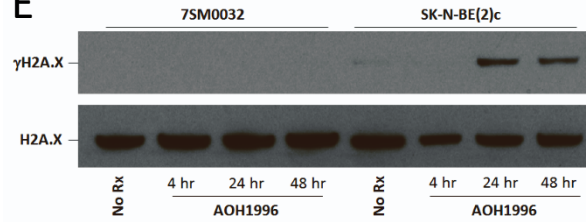
C



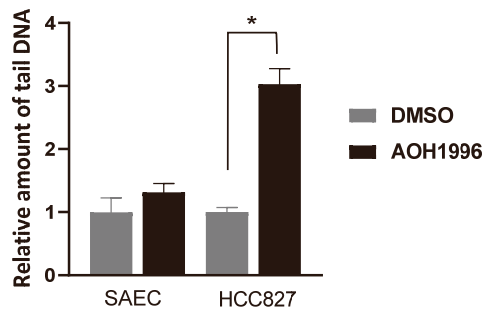
D



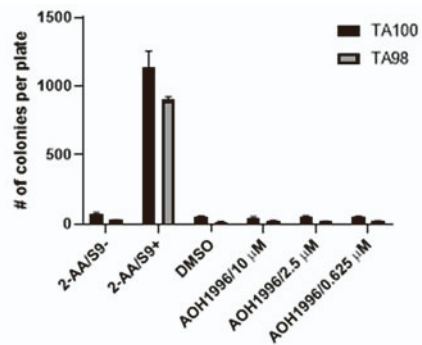
E



F



G



Supplemental Figure S6 (related to Figure 3): Selective inhibition of cancer cells

and mutagenicity: A) Cancer cells of the NCI60 panel were incubated in the presence of various concentrations of AOH1996 for 48 hours. Cells growth was analyzed by a sulforhodamine B (SRB) assay after cells were fixed by ice-cold 10% trichloroacetic acid (TCA). The GI_{50} in molar for each cell line was calculated by NCI (see method for details). **B-D)** Shown in the graph are the $\text{Log}GI_{50}$. As indicated in the figure, small cell lung cancer (**B**: H-82, H-524, H-526, LX22, and LX33), neuroblastoma (**C**: SK-N-BE(2)c, SH-SY5Y, and SK-N-AS), and prostate cancer (**D**: LN-caP, LN-caP-R, 22RV1, H660, LASCPC, PC3, and DU145) cell lines were treated with various concentrations of AOH1996 for 72 hours. Non-malignant cells (**B**: hSAEC and PBMC; and **C**: 7SM0032) were used as control. Cell growth was measured by the CellTiter-Glo® Luminescent assay. Relative cell growth in triplicate was averaged and graphed \pm S.D. **E)** Histone H2A.X and γ H2A.X in whole cell lysates from the indicated cells were analyzed by Western blot after treatment with 500 nM AOH1996 for various time. **F)** The normal lung small airway epithelial cells (SAEC) and the HCC827 lung adenocarcinoma cells were treated with DMSO or 500 nM AOH1996 for 72 hours. Following treatment, an alkaline comet assay was performed to determine the prevalence of single- and double-strand DNA breaks. The comet assay was performed using a commercially available kit (Bio-Techne, Minneapolis, MN) according to the manufacturer's instruction. The average amount of tail DNAs (measured by the software OpenComet, www.cometbio.org) in 166 individual AOH1996 treated cells were normalized to that in DMSO treated cells and graphed plus/minus SE. * $p < 0.01$. **G)** The potential genotoxicity of AOH1996 was

measured in an Ames test using the Salmonella Mutagenicity Test Kit purchased from MOLTOX[®] Molecular Toxicology Inc. (Boone, NC) according to manufacturer's instruction. The growth of the tester strains in histidine-deficient media depends on certain types of DNA mutations that restore their ability to synthesize histidine: frameshift mutation for TA98 (*rfa*, *uvrB*, *hisD*) and base pair substitution mutation for TA100 (*rfa*, *uvrB*, *hisG*), respectively. The number of bacterial colonies formed in histidine-deficient media, therefore, correlates positively to the rate of DNA mutations. The tester bacteria were treated with DMSO or AOH1996 in triplicates before being plated on to histidine-deficient media. The 2-aminoanthracene was used as positive control. The 2-aminoanthracene is a promutagen, which can be activated by the rat liver S9 fraction. The number of bacterial colonies of each tester strain under the indicated treatment conditions were averaged and graphed plus/minus SD.